NASA TECHNICAL NOTE

NASA TN D-5543

NASA TN D-5543

AN EXPERIMENTAL INVESTIGATION OF THE VELOCITY FLUCTUATIONS BEHIND OSCILLATING VANES

by Donald A. Buell

Ames Research Center
Moffett Field, Calif.

NATIONAL AERONAUTICS AND SPACE ADMINISTRATION • WASHINGTON, D. C. • NOVEMBER 1969

1. Report No. NASA TN D-5543	2. Government Accession No.	3. Recipient's Catalog No.
4. Title and Subtitle AN EXPERIMENTAL INVESTIGATION OF THE VELOCITY FLUCTUATIONS BEHIND OSCILLATING VANES		5. Report Date November 1969 6. Performing Organization Code
7. Author(s) Donald A. Buell		8. Performing Organization Report No. A-3361
9. Performing Organization Name and Address NASA Ames Research Center Moffett Field, California 94035		10. Work Unit No. 124-08-04-07-00-21 11. Contract or Grant No. 13. Type of Report and Period Covered TECHNICAL NOTE
12. Sponsoring Agency Name and Address National Aeronautics and Space Administration Washington D. C. 20546		14. Sponsoring Agency Code

15. Supplementary Notes

16. Abstract

Vortices were generated in a low-speed airstream by arrays of constant-chord vanes oscillating with amplitudes up to 16°. The resulting gusts at the center of the channel downstream from the vanes were predominantly lateral or longitudinal depending upon the phase and arrangement of the vanes. The maximum gust amplitudes near the centerline of the channel were over 45% of the free-stream velocity in both directions. The lateral extent of the gusts, especially the longitudinal gusts, was limited, and vane configurations that would improve the lateral distribution were investigated. Selected components of the fluctuations were analyzed for spectral content.

17. Key Words Suggested by Author	18. Distribution Statement		
Vortex Gust Generator Vanes	UNCLASSIFIED - UNLIMITED		
19. Security Classif. (of this report) UNCLASSIFIED	20. Security Classif. (of this page) UNCLASSIFIED	21. No. of Pages 54	22. Price* $3.00

*For sale by the Clearinghouse for Federal Scientific and Technical Information
Springfield, Virginia 22151

AN EXPERIMENTAL INVESTIGATION OF THE VELOCITY FLUCTUATIONS BEHIND OSCILLATING VANES

By Donald A. Buell

Ames Research Center

SUMMARY

Vortices were generated in a low-speed airstream by arrays of constant-chord vanes oscillating with amplitudes up to 16°. The resulting gusts at the center of the channel downstream from the vanes were predominantly lateral or longitudinal depending upon the phase and arrangement of the vanes. The maximum gust amplitudes near the centerline of the channel were over 45% of the free-stream velocity in both directions. The lateral extent of the gusts, especially the longitudinal gusts, was limited, and vane configurations that would improve the lateral distribution were investigated. Selected components of the fluctuations were analyzed for spectral content.

INTRODUCTION

The investigation described herein was a preliminary step in the development of a gust generator for a wind tunnel. Generating gusts in a wind tunnel makes it possible to simulate ground winds for studying the dynamic loads on high-drag structures exposed to the wind. In the past, turbulence has been added by means of grids (e.g., ref. 1), by developing a large boundary layer in an unusually long test section (as in ref. 2), and by using air ejectors (refs. 3 and 4 are recent examples). However, it has not yet proved feasible to reproduce simultaneously the large Reynolds numbers and turbulence scales appropriate for large structures. For this reason, other means of producing turbulence were sought, and moving vanes were thought to be potentially applicable to the problem. The purpose of the present tests was to establish the magnitude of, and the ability to control independently, the lateral and longitudinal velocity fluctuations behind oscillating vanes.

Oscillating vanes have been used by a number of investigators to generate velocity fluctuations, primarily in the lateral direction. For example, Hakkinen and Richardson report tests (ref. 5) of an airfoil which spanned the tunnel and oscillated in a lateral direction at rather modest amplitudes. Reid and Wrestler (ref. 6) used the tip vortices from pitching biplane vanes as the source of lateral gusts. Garby et al. (ref. 7) reported a more intense lateral gust behind a cascade of pitching airfoils.

The tests described in the present report represent an extension of the cascade concept, with the additional goal of producing longitudinal gusts by means of appropriate phase relationships between the airfoils.

Prior to the experimental work, a digital computer program was written which would approximately simulate the flow and would thus be an aid to test organization. Plots of computed flow velocities proved to be helpful in visualizing the flow and are included in the report. The computing scheme is described briefly in an appendix.

NOTATION

a	image-vortex spacing in computer simulation, ft
B	bandwidth of spectrum analysis, Hz
c	vane chord, ft
C_L	lift coefficient, $\frac{\text{lift per unit span}}{(1/2)\rho U^2 c}$
f	frequency of vane oscillation, Hz
f_a	frequency of spectrum analyzer, Hz
H	distance between floor and ceiling of test section, ft
n	integer
s	horizontal and vertical spacing between 1/4-chord points of vanes, ft
t	time, sec
u	increment in longitudinal velocity, fps
U	free-stream velocity, fps
U_{axial}	velocity along probe axis, fps
$U_\perp$	velocity perpendicular to probe axis, fps
v	velocity perpendicular to tunnel axis and vane hinge line, fps
x,y	longitudinal and lateral coordinates, ft
α	angle of attack of vane, deg
α_{av}	"average" angle of attack of vane, $\frac{1}{2}(\alpha_{max} + \alpha_{min})$, deg
α_r	angle of attack of vane, rad
Γ	vortex strength, ft^2/sec

Δ increment

ζ,η longitudinal and lateral vortex-to-probe coordinates in computer simulation, ft

ρ free-stream density, slugs/ft^3

ϕ phase lag of gust, relative to angle of attack of downstream vanes below center line, cycles

$\Phi_{u/U}$ power spectral density of longitudinal gust, $\frac{1}{B}\overline{\left(\frac{u}{U}\right)_a^2}$, per Hz

$\Phi_{v/U}$ power spectral density of lateral gust, $\frac{1}{B}\overline{\left(\frac{v}{U}\right)_a^2}$, per Hz

$\overline{(\ )}$ time average of ( )

Subscripts

a that portion fluctuating at $f_a \pm \frac{B}{2}$

b bound vortex

max maximum

min minimum

t trailing vortex

u gust velocity u, or uncorrected for vane-linkage distortion

v gust velocity v or vortex

APPARATUS

Vanes and Drive Equipment

Vanes with constant-chord NACA 0015 airfoil sections were constructed from mahogany with aluminum-angle spars and a fiberglas and resin covering. The vanes were mounted in various numbers and arrangements between aluminum walls in rows and columns approximately one chord length apart, as indicated in figure 1. A channel was formed around the vanes by a wooden ceiling and floor approximately one chord length above and below the vane array. The entire system was installed in a 7- by 10-foot wind-tunnel section along with the mechanism to oscillate each vane in pitch about the quarter-chord point. Side fairings were installed to screen the airflow from the oscillation

mechanism. Figure 2 is a view of the installation from the upstream direction. Any or all of the vanes were removable so as to provide a variety of configurations for the tests.

The vanes were driven by a 125-horsepower 6-pole induction motor, which is visible at the lower front part of figure 2. The objects behind the motor are shafts that connected cranks below each end of the vanes. The motor power was transmitted to the cranks through "silent" chains. The cranks then converted the rotary motion to the oscillating motion transmitted to the vanes. The vane pitching was approximately sinusoidal with time. Deviations from a precise sinusoidal motion were caused partly by linkage design and partly by distortion of the linkage when large loads were transmitted.

The length of the linkage elements was adjustable, so that the pitching amplitude and the average angle of attack of each vane could be adjusted individually. The maximum and minimum angles of attack of each vane at each frequency were checked (with the wind off) by direct observation of the displacement of the trailing edge of the vane. The measurements were repeatable to within 10 percent or 1°, whichever was larger, over the complete frequency range.

Velocity and Torque-Measuring Equipment

Cross wires were used to sense the velocity fluctuations downstream from the vanes. The wires were mounted in a probe as shown in figure 3. There were two probes, each supported by a horizontal tube, which can be seen in figure 4. The tube positions were manually adjustable in the streamwise direction and in the lateral direction along either the vertical or horizontal centerlines of the channel cross section. For the more upstream locations, the tubes were supported by an additional steel strut so that the natural frequency of the support system would alway be higher than the vane frequency.

The hot wires were connected to the following electronic equipment: four units which supplied current to the wires and, by means of a feedback circuit, maintained an approximately constant resistance 1.7 times the cold-wire resistance; four linearizers which squared the wire outputs twice; and two sum and difference circuits. The sum and difference voltages were fed to an oscillograph and a tape recorder.

The outputs of each pair of wires were combined to give the velocity along, and perpendicular to, the axis of the probe, according to the following approximate relationships:

$$U_{axial} \text{ is proportional to } (O_1 + O_2)$$

$$U_1 \text{ is proportional to } (O_1 - O_2)$$

$$O_1 = [V_1^2 - (V_{1,U=0})^2]^2 = \text{output from linearizer no. 1}$$

$$O_2 = [V_2^2 - (V_{2,U=0})^2]^2 = \text{output from linearizer no. 2}$$

V_1 = voltage across a precision resistor due to current from wire no. 1

V_2 = voltage across a precision resistor due to current from wire no. 2

The above relationships are approximate for a multitude of reasons which are noted in various sources (e.g., ref. 8). In particular, the velocity normally changes by more than the fourth power of the wire voltage at the higher velocities. Additional circuitry was included in the linearizer to compensate partially for this loss of wire sensitivity. A typical calibration is shown in figure 5. The hot wires were used only to record velocity fluctuations about selected average axial velocities. Used in this manner, the anemometer output was sufficiently linear to cause negligible distortion to the wave form.

The dynamic response of the hot-wire system was indirectly evaluated by inserting a square-wave signal into the hot-wire circuit and observing its speed of recovery at each half-cycle. It was thus determined that the response would be attenuated less than 30 percent at 10,000 Hz. Since such high frequencies were not anticipated, the wire outputs were passed through a 1000-Hz filter which caused less than 2-percent attenuation below 200-Hz and reduced electronic noise to a negligible amplitude.

A pitot tube was mounted downstream from the vanes for purposes of velocity calibration. The pitot head was located 7 inches below and 3 inches to the side of the tunnel centerline, and 16 inches behind the hinge line of the aft-most vanes (fig. 1). The vertical tube which supported the pitot head is visible in figure 4.

The torque to the vanes was measured by means of strain gages mounted on a connecting shaft. This information was intended to indicate vane position, but mechanical looseness distorted the wave shape. The data could be used as intended only at the higher frequencies where the maximum inertial strain coincident with the maximum vane deflection could be clearly identified.

TESTS

Various arrangements of vanes were tested and are summarized in table I. The three main categories denote the direction of the expected gust on the channel centerline downstream from the vanes. That is, the lateral-gust configurations had the vanes in each column in phase with each other so that the velocity fluctuation on the channel centerline would be primarily in the lateral direction. In the longitudinal-gust configurations, the vanes on one side of the centerline were 180° out of phase with those on the opposite side, resulting in longitudinal velocity fluctuations on the centerline. The asymmetrical configurations produced gusts in both directions.

For most of the tests the amplitude of the vane oscillation was as large as possible (up to 16°) without incurring severe flow separation, and the average angle of attack was zero. The corresponding oscillation frequencies were from 1 to 15 Hz. A few tests were conducted with the vanes oscillating at small amplitudes about various average angles of attack. The range of oscillation frequencies for the small amplitude tests was extended to 30 Hz.

The usual test procedure, after adjustment of the amplitude and average angle of attack, was to set the desired average channel velocity and then record the hot-wire-anemometer outputs at various frequencies of vane oscillation. The average channel velocity was determined from the wind-tunnel manometer, which had been calibrated previously with no vane movement by means of the pitot tube. The average velocity was set between 50 and 250 feet per second. The vane oscillation did not seem to affect the wind-tunnel power requirements or otherwise alter the tunnel operating characteristics.

CORRECTIONS

Bending of the vane-driving linkage caused the oscillation amplitude to increase with frequency, thus complicating data analysis. On the assumption (later evaluated) that the gusts were proportional to vane amplitude, the gusts were corrected to make them correspond to the low-frequency amplitude. This correction amounted to a maximum of 11 percent for the large amplitudes and 50 percent for the small amplitude high-frequency points. An error in the method exists because the vane amplitudes were known for the wind-off condition only. It is estimated from the torque data that the wind altered the vane amplitudes by as much as 3 percent for large amplitudes and 15 percent for small amplitudes. This error, occurring at high free-stream velocities, was ignored since it was rarely significant.

Errors in gust measurement arose from changes in sensitivity of the hot-wire system as tunnel and instrumentation temperatures drifted. To compensate for these errors, the average axial velocities from the hot-wire system were compared to those from the tunnel manometer system during each test, and the sensitivities to both axial and lateral gusts were then adjusted. The validity of this procedure was checked by applying it to repeat calibrations of the hot wires at various times throughout the investigation. It was indicated that the inaccuracy remaining was a scatter of individual readings due partially to manometer friction. The maximum error was 15 percent at 50 feet per second, decreasing to 5 percent at 250 feet per second. Another error in gust amplitude occurred because the amplitude was measured from a time history that was not exactly sinusoidal. An effort was made to eliminate frequencies higher than the fundamental from the amplitude measurement, but of course this became difficult when the wave shape was very distorted.

In summary, corrections have been made to reduce the systematic errors involved, but a number of inaccuracies remain, primarily in the form of data scatter. These are most serious at low speeds and small amplitudes.

SPECTRAL ANALYSIS

The frequency content of some of the velocity time histories was obtained on an electrical-analog power-spectrum analyzer. This equipment in effect measured the average power within a 1.25 Hz bandwidth at various center frequencies. A 1-minute sample of data was continuously analyzed while the center frequency was changing at the rate of 0.1 Hz per second. The output was smoothed with a circuit having a time constant of 4 seconds. This is somewhat low for good statistical accuracy but gave a better resolution of discrete frequencies, which are the main content of the data.

The resulting analyzer output is shown in figure 6 for a 25-Hz calibration input with a root-mean-square amplitude of 0.5 V. The flat top at the peak of the curve is characteristic of the particular analyzer used.

RESULTS

Sketches of the vortices in the flow field from the computer studies are presented in figures 7 to 9. The results of the gust measurements are presented as follows: time histories in figures 10 to 13, amplitudes in figures 14 to 26, phase angles in figures 27 to 29, and power spectra in figures 30 to 36.

The vortex sketches illustrate the rolling-up process. The time histories and spectra provide a means of assessing the wave distortion as compared to a sine wave. The amplitudes and phase angles furnish the basic information of the tests, although one must resort to spectra for amplitude information when the wave shape is very distorted.

In the presentation of the result the "average" angle of attack is taken as the angle midway between maximum and minimum angles of attack and is zero unless otherwise noted. When the distance behind the vanes is specified, it has been measured from the trailing edge of the downstream vanes.

DISCUSSION

Vortex Sketches

The velocity fluctuations behind a moving vane result from changes in strength of the bound vortex and also from the vorticity which moves downstream after having been shed from the vane. The underlying vortex structure is pictured in figures 7 to 9 as it was computed for a given instant of time. The symbols in these figures represent point vortices that have been shed from the vanes. The lines from each symbol represent a velocity vector that would be measured by an observer moving with the main air mass at the

velocity U. The identifying frequency parameter fs/U is formed from the wave number f/U, which was systematically varied during the investigation, and a representative vane dimension, chosen arbitrarily to be the spacing s. The figures show the point vortices coalescing into large trailing vortices at the higher values of fs/U, where the energy in the shed vorticity is large.

The shaded area in these figures connects the point vortices that have been shed from the two inner vanes in the downstream column. This area therefore has a shape that smoke filaments would assume if the smoke were discharged from between the two vanes. This pattern is the so-called streak line (which is neither a streamline nor a particle path in this situation). Bratt presents smoke pictures in reference 9, taken behind a single oscillating airfoil, which are similar to the computed sketches in figures 7 and 8.

The vane configuration in figures 7 and 8 is identified as a lateral-gust configuration because a point on the centerline of the channel experiences gusts in the lateral direction as the vortices pass by. It is apparent that the same vane configuration also produces longitudinal gusts at points off the centerline. The so-called longitudinal-gust configuration sketched in figure 9 produces pairs of counterrotating vortices that produce longitudinal gusts on the centerline. The confusion in the pattern at fs/U of 0.150 (fig. 9) is associated with a loss of effectiveness in producing gusts which will be pointed out in the experimental data. The computer simulation indicated that all of the vane configurations would experience a loss of effectiveness if fs/U were increased sufficiently. Computations for configurations without walls indicated that the proximity of the walls was not a major factor in the loss of effectiveness.

Time Histories

Samples of the time histories of velocities actually measured behind the oscillating vanes are presented in figures 10 to 13. The time histories shown are for various vane frequencies and free-stream velocities. Figures 10 and 11 compare measurements made on the centerline with those near the wall; figures 12 and 13 compare centerline measurements at two distances behind the vanes. The passage of the large vortices past the probe is indicated by the large amplitude waves that occur at the vane frequency.

Referring to the traces of lateral velocity v on the left side of figure 10, one can see that the fundamental wave shape is not absolutely sinusoidal. This departure from the desired wave shape was not caused by aerodynamic phenomena but, according to calculations, was the result of vane-linkage design and bending. Other distortions, such as the sideways tilt of the longitudinal-velocity (u) waves on the left side of figure 11, were caused by self-induced distortions of the vortex system. Other investigators (e.g., ref. 10) have observed similar "sawtooth" waveforms in high-amplitude longitudinal waves.

Higher frequencies, such as those in u on the left side of figure 10, tended to be multiples of the fundamental. These fluctuations could result

from vane wakes. The edges of the shaded area in figure 8, for example, would represent the centers of the wakes from the two inner vanes. One can see that a probe on the centerline would feel the wakes from these two inner vanes four times during each cycle and that wakes from other vanes would cross the probe if fs/U were large enough.

Data similar to figure 13 but for more widely separated probe positions (1.8 s and 7.8 s behind the vanes) were recorded simultaneously with a suitable spanwise separation of the probes. By measuring the phase shift, it was possible to determine that the vortices moved downstream at free-stream velocity, with an uncertainty (due to wave distortion, etc.) of less than 10 percent.

Gust Amplitudes

Lateral-gust configuration.- The ratio of gust velocity to free-stream velocity is plotted in figures 14 to 26 versus the reduced frequency parameter fs/U. Since the strength of the vortex elements shed from the vanes is proportional to the rate of change of the vane lift, one might expect the velocities induced by the trailing vortices to increase with vane frequency. Figure 14 shows that such is the case for the configuration shown. To within the accuracy of the experiment, straight lines appear to fit measurements over a wide range of free-stream velocities.

The three lower sets of data in figure 14 represent gusts at various distances behind the vanes. The intercept of each line with the vertical axis is the gust amplitude from the bound vortices at the vanes, since there are no trailing vortices at zero frequency. It can be verified from the figure that the intercept varies approximately inversely with distance behind the 1/4-chord point, as would be expected from simple vortex theory. The slope of the lines is nearly proportional to the distance behind the trailing edge. At high values of fs/U the net effect was an increase in gust amplitude as the probe was moved downstream. Such an effect contrasts with the decay process that would be expected further downstream.

An increase in α_{max} from 10° to 15° (fig. 14) increased the intercept of the faired line in proportion to α_{max}, within the accuracy of angle measurement. However, the slope was increased by a considerably greater proportion. This latter effect and other results discussed later in the report indicate that the vorticity shed from the vanes was not proportional to amplitude, as had been anticipated.

The inverse proportionality of intercept to downstream distance is again applicable to 2 columns of vanes in phase (fig. 15) if the distances are measured from the 1/4-chord point of the downstream vanes (which defines the effective location of the bound vortices). The slopes are likewise proportional to distance downstream except for the position very close to the vanes, where the slope was higher. The change in amplitude afforded by the addition of a column of vanes can be roughly assessed by comparing the single-column data for $\alpha_{max} = 15°$ in figure 14 with the double-column data

of figure 15, 4.8 s behind the vanes. It may be seen that the second column hardly changed the intercept and increased the slope about 50 percent. With the double-column vanes the maximum lateral gust measured was over 45 percent of the free-stream velocity.

The effect of phase differences between front and rear columns was briefly investigated and found to be rather minor. Figure 15 shows that the most extreme phase difference tested, 90°, reduced the intercept about 10 percent and the slope about 20 percent.

Samples of the gust amplitudes near the wall are shown in figure 16. It is evident that the gusts near the wall are predominantly longitudinal.

The results from tests with an increased frequency range are shown in figure 17. The data are scattered considerably from the single straight-line relationship previously observed, but it can be shown that the scatter generally follows a pattern. Solid lines have been faired along the lower bounds of the data and adequately represent the low-frequency points; dashed lines define the upper limit of the spread in data and usually pass through the highest frequency points. The reason for this variance can be traced to the gust correction which was based on the assumption that gust amplitude increases with vane amplitude and that all data should be made to correspond to the vane amplitude at low frequency. The correction was apparently insufficient, and the insufficiency became evident in this case because the change in vane amplitude was so large (100 percent).

In order to define the relationship of vane amplitude and gust amplitude correctly, the uncorrected data were plotted in a manner similar to figure 17, and the slopes of the lines through high and low frequency points were measured. These slopes are presented in figure 18 versus the measured vane amplitude, averaged between the front and rear columns. The slopes represent the effectiveness of the shed vorticity in producing gusts. It can be seen for widely differing average vane angles and probe positions that the effectiveness in producing gusts approaches zero while the vane amplitudes are still finite. Of course, the bound vortices also produce gusts as defined by the intercepts for zero frequency in figures 15 and 17. Gusts from this source are approximately proportional to vane amplitude.

The measurements indicated in figure 17 for $\alpha_{av} = 0$ were repeated at a position 1.5s below the centerline. There was no significant difference between these results and those of figure 17.

Lateral-gust amplitudes for a considerably different vane configuration are presented in figure 19. At the rearmost probe position, the initial slope of the data fairing falls very nearly in line with the slopes for the two-column configuration (fig. 18), but the intercept is roughly half that for the two-column configuration. In addition, there is an obvious loss of effectiveness at high values of fs/U. The net result is that the 24 vanes in configuration C produced less than one-half as large a maximum gust on the centerline as the 12 vanes in two columns.

Longitudinal-gust configuration.- Longitudinal gusts produced on the centerline by one and two columns of vanes in a longitudinal-gust configuration are shown in figures 20 and 21. The lines defined by the data points had much smaller intercepts but much larger initial slopes than the lines through the lateral-gust data for comparable lateral-gust configurations (figs. 14 and 15). In addition, the slopes changed sharply at an fs/U of about 0.06. By coincidence, the maximum longitudinal gust obtained in the tests (fig. 21) was about equal to the maximum lateral gust (fig. 15). Another point of interest in figure 21 is that the insertion of stationary vanes downstream from the oscillating vanes greatly reduced the gusts farther downstream but had only minor effects at points between the two sets of vanes.

As noted previously, the longitudinal gusts were the result of pairs of counterrotating vortices. Since each vortex spanned only half the height of the test section, one might expect that the longitudinal gusts would be nearly zero half way between the centerline and the wall, and this was found to be true. Consequently, other configurations (fig. 22) were tested with the aim of broadening the lateral distance over which the longitudinal gust would be reasonably constant. The upper four-vane configuration in figure 22 produced a large gust at the centerline - about 60 percent of that from the full two columns - but it is apparent that the gust is much smaller at 1.5 s below the centerline. In fact, the latter gust was 180° out of phase with the centerline gust. It is obvious that the vortices from the two lower vanes passed between the two probe positions. The remaining two configurations have a better lateral distribution at the expense of producing considerably smaller gusts.

Figure 23 shows that the undesired lateral gust is large at the measuring positions below the centerline. Although not shown, lateral gusts on the centerline were generally small.

Figure 24 presents data for small vane amplitudes and high frequencies. The nature of the curves makes it difficult to ascertain the effect of vane amplitude, as was done for the lateral-gust configuration. The maximum longitudinal gusts for the eight vane configuration in figures 22 and 24 do appear to be proportional to vane amplitude.

In an attempt to increase the longitudinal gust, a configuration with 24 vanes was tested with the results shown in figure 25. The top set of data when compared with the lower set of data in figure 22 shows that the additional vanes about doubled the gusts at fs/U up to 0.04.

Asymmetric configurations.- Figure 26 shows data for one column with only half of the vanes moving. The lateral gusts were very nearly half those induced by a full column of vanes oscillating in phase (fig. 14), and the longitudinal gusts were slightly over half of those induced by a full-column longitudinal-gust configuration (fig. 20). (In making the latter comparison, it was assumed that the gusts were proportional to the vane amplitude.)

Phase Angles

Phase information must be added to amplitude information to describe a fluctuation. Figure 27 shows typical values of the phase lag ϕ_v for various probe locations, vane amplitudes, and phase differences between two columns of vanes in a lateral-gust configuration. The parameter ϕ_v is the phase of the lateral-velocity fluctuation subtracted from the phase of the pitching oscillation of the downstream vanes. The figure shows that lines through the data very nearly follow the relationship

$$\phi_v = 0.5 + \frac{fs}{U}\left(\frac{\Delta x}{s}\right)$$

where Δx is the distance from trailing edge of downstream vanes to the probe.

A simple interpretation of this result can be derived by assuming that another probe exists a distance d upstream of the actual probe. If the vortices travel at a velocity U, as previously observed, it takes a period of time $\Delta t = d/U$ for the vortices to travel from one probe to the other. In that time the phase of the downstream probe would lag the phase of the upstream probe by $f\,\Delta t$ cycles which equals

$$\frac{fd}{U} = \frac{fs}{U}\,\frac{d}{s}$$

The phase at the downstream probe would then be

$$\phi_v = \left(\phi_v\right)_{\text{upstream}} + \frac{fs}{U}\left(\frac{d}{s}\right)$$

This expression would take the same form as that actually observed if the hypothetical upstream probe were at the trailing edge of the downstream vanes ($d = \Delta x$) and if the velocity fluctuations at that point always lagged the angle of attack of the downstream vanes by 1/2 cycle regardless of frequency, free-stream velocity, vane amplitude, or phase angle of the upstream vanes. The fulfillment of these conditions suggests that the trailing vortices were, in effect, formed at the trailing edge of the downstream vanes.

Examples of phase-angle data for other configurations are presented in figures 28 and 29. The longitudinal gusts downstream from the vane arrays invariably had phase lags with larger slopes and smaller intercepts than indicated by the above expression.

Gust Spectra

Figures 30 to 36 present power spectra of a very limited number of velocity time histories to show the energy distribution between the longitudinal and lateral velocity fluctuations. It should be noted that many of the spectra have been amplified by a factor of 10 to make the peaks clearly visible. Those small peaks which have considerably smaller bandwidths than the large peaks were mostly unrepeatable and should be disregarded.

Spectra for single-column configurations operating at large amplitudes are shown in figures 30 to 33. Spectra of the velocities in the intended gust directions have a large peak at the vane frequency and very often have small peaks at twice the vane frequency. The latter peaks are a manifestation of the distortion of the sinusoidal wave form and involve a modest amount of energy, usually 5 percent or less of the energy in the predominant peak. Small spectral peaks (magnified in the figures) can also be seen for the velocity component perpendicular to the intended gust direction.

Spectra for the vanes oscillating at small amplitudes are shown in figures 34 to 36. Although the vanes were intended to generate lateral gusts only, the longitudinal gusts on the centerline and 1.5 s below the centerline had spectral peaks as high as 10 and 50 percent, respectively, of the lateral-gust energy.

CONCLUDING REMARKS

Velocity measurements downstream from oscillating vanes have demonstrated that gusts of over 45 percent of the free-stream velocity can be generated in either a lateral or longitudinal direction. However, it was generally not possible to limit the gusts to only one direction over a significant portion of the airstream. That is, the goal of completely controlling the gust direction was not realized. In addition, large longitudinal gusts could be generated over only a small portion of the airstream near the centerline. It appears, therefore, that oscillating vanes would not be suitable for synthesizing two- or three-dimensional gusts representative of atmospheric turbulence.

Ames Research Center
National Aeronautics and Space Administration
Moffett Field, Calif. 94035, July 11, 1969

APPENDIX

COMPUTER SIMULATION

A precise computation of the flow field is beyond the scope of this investigation. However, it was deemed useful to have a rough estimate of the velocities induced by various vane configurations to help in test planning, and a program was written for this purpose. The flow was considered to be two-dimensional and potential. Point vortices were inserted into the flow to represent the vorticity actually generated by the vanes. The changes in angle of attack induced at the vanes were neglected to save computer time, and the effective amplitude of the vanes was thus in error. In the case of two columns of vanes, for which the flow field plots are presented, the error was subsequently evaluated by comparison with experimental data. The computed gusts were found to be high by the order of 50 percent for most frequencies.

The strength of the bound vortex which represented the vane lift was

$$\Gamma_b = (1/2)C_\ell Uc = (1/2)(2\pi\alpha_r\ 0.58)Uc$$

The value 0.58 was drawn from calculations for a cascade of airfoils (ref. 11) with no stagger or phase difference and zero frequency. It agrees approximately with extrapolation of cascade data from reference 12.

The angle of attack, and, hence, the bound-vortex strength, varied sinusoidally with time, requiring the introduction of trailing vortices of equal strength and opposite rotation. Each trailing vortex, produced at time intervals Δt, had the strength $\Gamma_t = -(d\Gamma_b/dt)\Delta t$ and was assumed to retain this strength thereafter. These vortices were assumed to proceed in straight lines with a velocity equal to the free-stream velocity plus increments induced by all other vortices in the flow field. After the next time interval, the velocities were again summed at each of the vortex positions, and the trailing vortices proceeded with a new speed and direction.

The presence of the tunnel walls was simulated in the conventional manner by an infinite column of image vortices added outside the walls for each vortex in the flow field so that the induced velocities perpendicular to the walls would be zero. In effect, this amounts to the addition of one column of image vortices of the same rotation as the real vortex at positions x_V, $y_V \pm n2H$ and a second column of image vortices of opposite rotation at positions x_V, $H\text{-}y_V \pm (n - 1)2H$, where x_V and y_V are coordinates of the real vortex ($y_V = 0$ on the tunnel centerline), n is an integer which goes from 1 to ∞, and H is height of the tunnel. The sum of the velocities induced at (x,y) by the point vortex and its associated images can be expressed in the following form, similar to that in reference 13.

$$\Delta u = \frac{\Gamma}{2a} \frac{\sin[2\pi(\eta/a)]}{\cosh[2\pi(\zeta/a)] - \cos[2\pi(\eta/a)]}$$

$$\Delta v = \frac{\Gamma}{2a} \frac{\sinh[2\pi(\zeta/a)]}{\cosh[2\pi(\zeta/a)] - \cos[2\pi(\eta/a)]}$$

where

$a = 2H$

$\zeta = x - x_v$

$\eta = y - y_v$ for the first column

$\eta = y - (H - y_v)$ for the second column

The time interval chosen was a compromise between a small value which would improve the accuracy and a large value which would decrease the computing time. In some cases a vortex landed nearly on top of another vortex and was lost after receiving a very large velocity increment. Of course, this could not happen if Δt were infinitesimal. It is apparent that all the velocity computations suffer similarly though to a smaller extent. Hence, the method is an approximation which tends to break down as more vortices or larger time intervals are required.

REFERENCES

1. Vickery, B. J.: On the Flow Behind a Coarse Grid and Its Use as a Model of Atmospheric Turbulence in Studies Related to Wind Loads on Buildings. NPL Aero Report 1143, 1965.

2. Plate, Erich J.; and Cermak, J. E.: Micrometeorological Wind Tunnel Facility. Colorado State University Report CER63EJP-JEC9, 1963.

3. Thomas, Richard E.; and Morland, Bruce T., Jr.: Final Report, Gust Simulation in a Wind Tunnel. Texas Engineering Experiment Station, Texas A & M University, Space Technology Report 67-52, 1967.

4. Teunissen, H. W.: An Ejector-Driven Wind Tunnel for the Generation of Turbulent Flows with Arbitrary Mean Velocity Profile. University of Toronto, Institute for Aerospace Studies Technical Note No. 133, 1969.

5. Hakkinen, Raimo J.; and Richardson, A. S., Jr.: Theoretical and Experimental Investigation of Random Gust Loads. Part I - Aerodynamic Transfer Function of a Simple Wing Configuration in Incompressible Flow. NACA TN 3878, 1957.

6. Reid, Charles F., Jr.; and Wrestler, Clifton G., Jr.: An Investigation of a Device to Oscillate a Wind-tunnel Airstream. NASA TN D-739, 1961.

7. Garby, L. C.; Kuethe, A. M.; and Schetzer, J. D.: The Generation of Gusts in a Wind Tunnel and Measurement of Unsteady Lift on an Airfoil. WADC Technical Report 57-401, 1957.

8. Grant, H. P.; and Kronauer, R. E.: Fundamentals of Hot Wire Anemometry. ASME Symposium on Measurements in Unsteady Flow, Worcester, Mass., May 21 - 23, 1962, pp. 44-53.

9. Bratt, J. B.: Flow Patterns in the Wake of an Oscillating Airfoil. Aeronautical Research Council, R & M No. 2773, 1953.

10. Truman, J. D.; and Lipstein, J. J.: A Study of Methods for Introducing Pressure Oscillations into a Gas Stream, with a Survey of Related Instrumentation. General Electric Report R51GL-127, 1951.

11. Whitehead, D. S.: Force and Moment Coefficients for Vibrating Aerofoils in Cascade. Ministry of Aviation Report TIL(BR)433, 1960.

12. Emery, James C.; Herrig, L. Joseph; Erwin, John R.; and Felix, A. Richard: Systematic Two-Dimensional Cascade Tests of NACA 65-Series Compressor Blades at Low Speeds. NACA TR 1368, 1958.

13. Lamb, Sir Horace: Hydrodynamics. Sixth ed., Dover Publications, 1945, Article 156.

TABLE I.- VANE ARRANGEMENTS AND ANGLES OF ATTACK

Gust direction	Configuration	Nominal α_{max}, deg	Vane location		Amplitude at low frequency, deg	α_{av}, deg
			Column	Row		
Lateral	A	15	1	1-6	15	0
Lateral	A	10	1	1-6	10	0
Lateral	B	13-1/2	1	1-6	12	0
			2	1-6	15	0
Lateral	B	3-1/2	1	1-6	3	0
			2	1-6	4	0
Lateral	B	14	1	1-6	3	9
			2	1-6	4	12
Lateral	C	12	1	1,2,5,6	12	0
			2	1,2,5,6	12	0
			3	1,2,5,6	12	0
			4	1,2,5,6	12	0
			5	1,2,5,6	12	0
			6	1,2,5,6	12	0
Longitudinal	D	12	1	1-6	12,13,10,10,13,12	0
Longitudinal	E	12-1/2	1	1-6	12,13,10,10,13,12	0
			2	1-6	12,16,12,12,16,12	
Longitudinal	F	12-1/2	1	1-6	12,13,10,10,13,12	0
			2	1-6	12,16,12,12,16,12	0
			5	1-6	0	0
			6	1-6	0	0
Longitudinal	G	11	1	3,4	10	0
			2	3,4	12	0
Longitudinal	H	12	1	1,6	12	0
			2	1,6	12	0
Longitudinal	J	12	1	1,2,5,6	12	0
			2	1,2,5,6	12	0
Longitudinal	J	4	1	1,2,5,6	4	0
			2	1,2,5,6	4	0
Longitudinal	J	12	1	1,2,5,6	3	9
			2	1,2,5,6	3	9
Longitudinal	K	12	1	1,2,5,6	12	0
			2	1,2,5,6	12	0
			3	1,2,5,6	12	0
			4	1,2,5,6	12	0
			5	1,2,5,6	12	0
			6	1,2,5,6	12	0
Asymmetric	L	7-1/2	1	1-6	0,0,0,15,15,15	0
Asymmetric	M	12	1	4	12	0

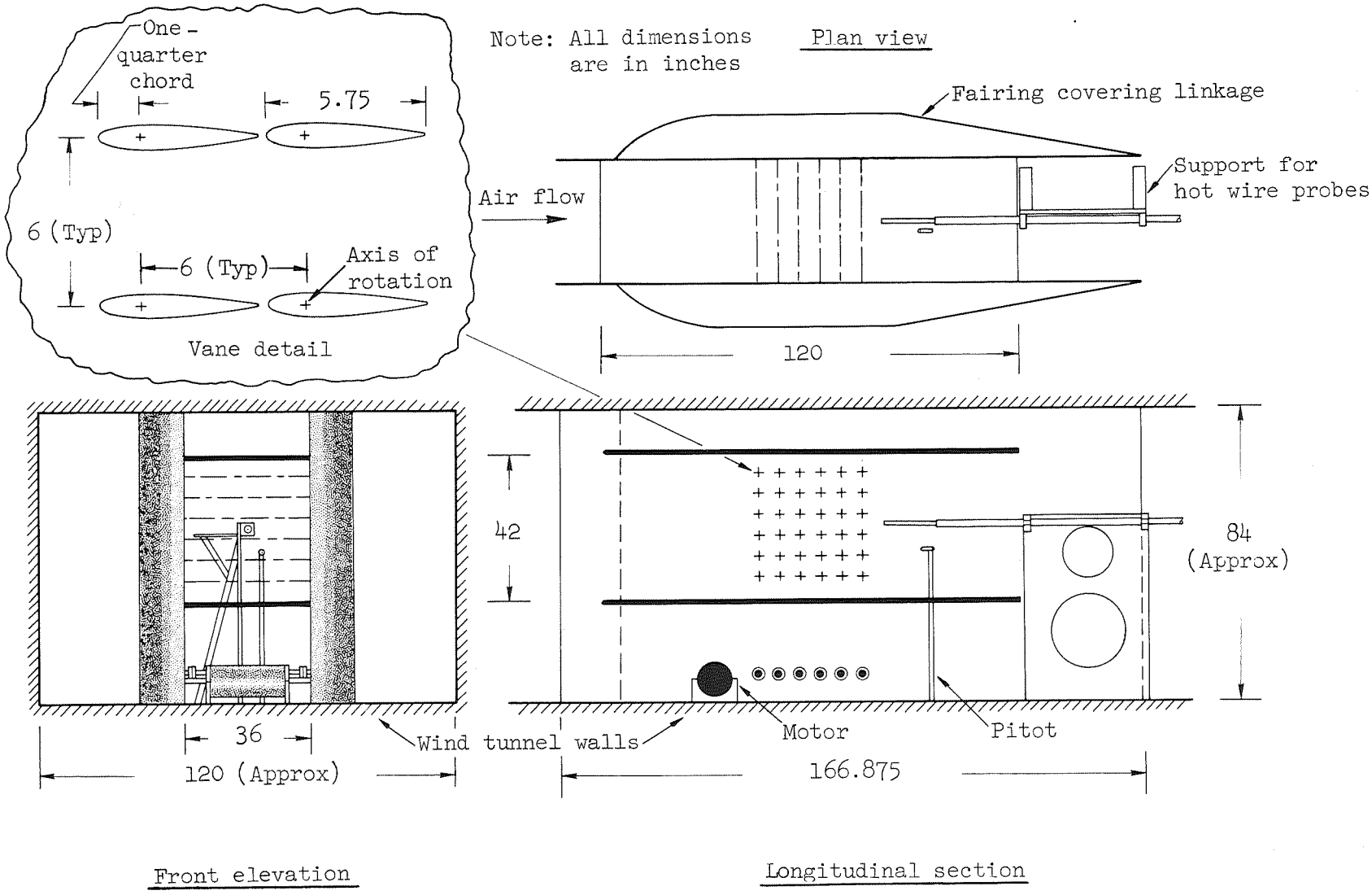

Figure 1.- Dimensional sketch of the gust-generating apparatus.

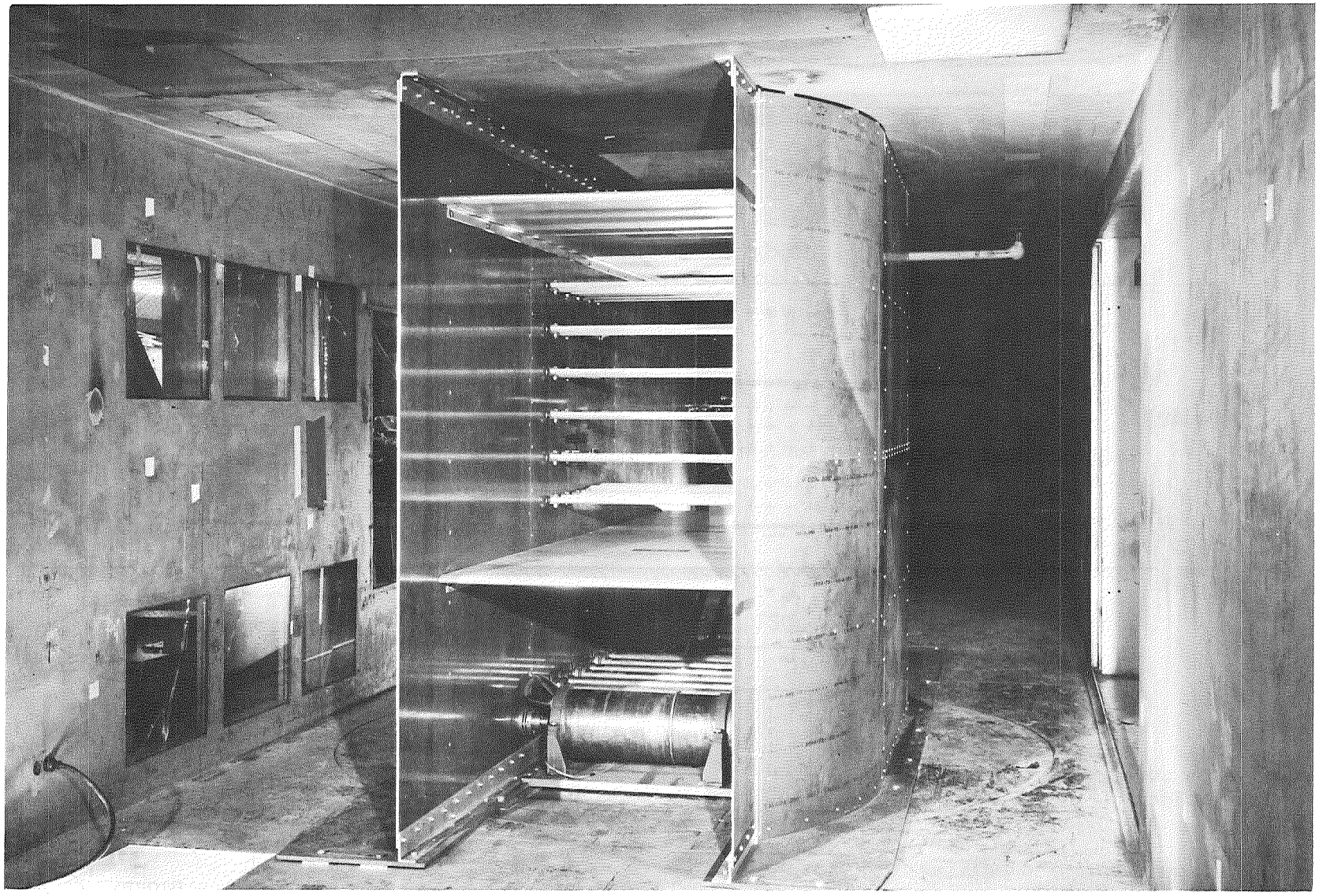

A-37374

Figure 2.- View from upstream of the gust-generating apparatus mounted in the wind tunnel.

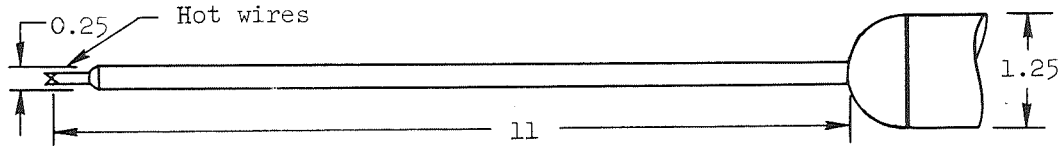

Hot-wire probe

Note: All linear dimensions
are in inches

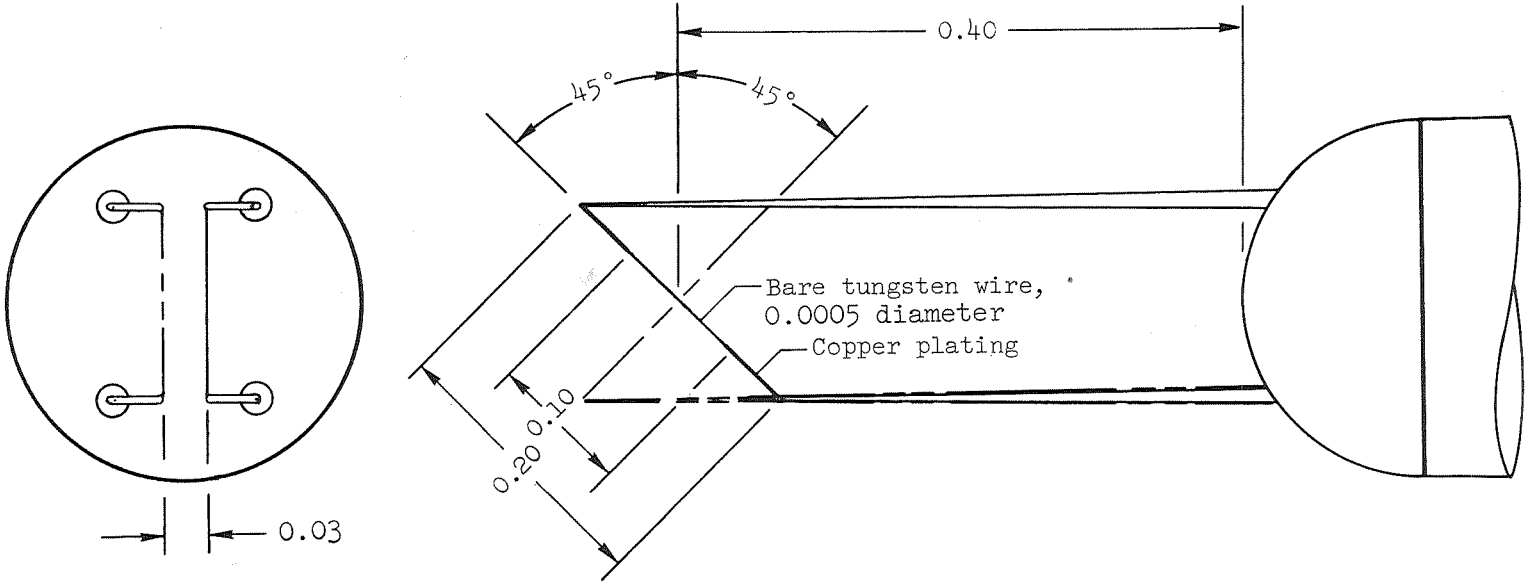

Enlarged view of hot wire

Figure 3.- Details of the upstream portion of a hot-wire probe.

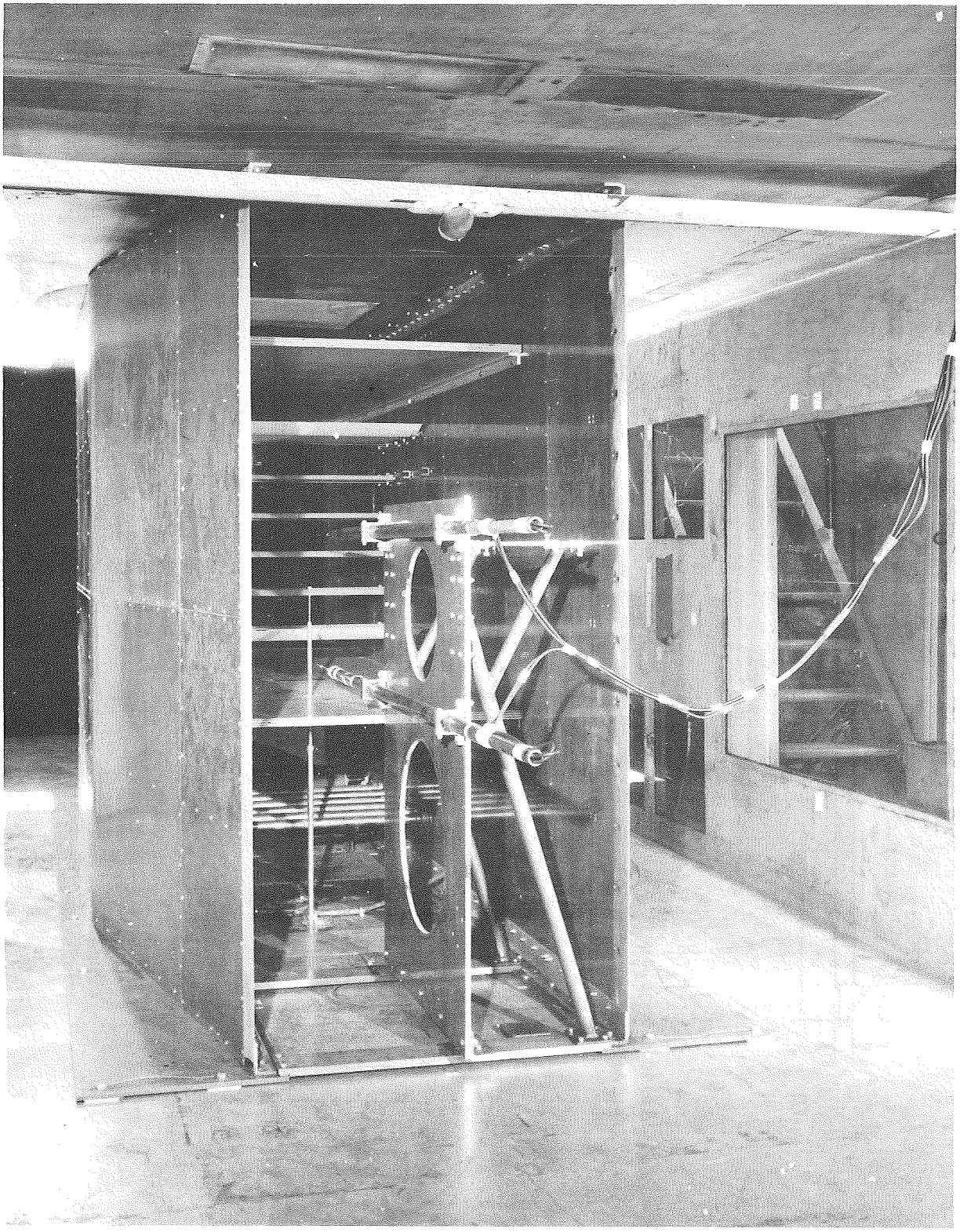

A-37375

Figure 4.- View from downstream of the gust-generating and measuring apparatus.

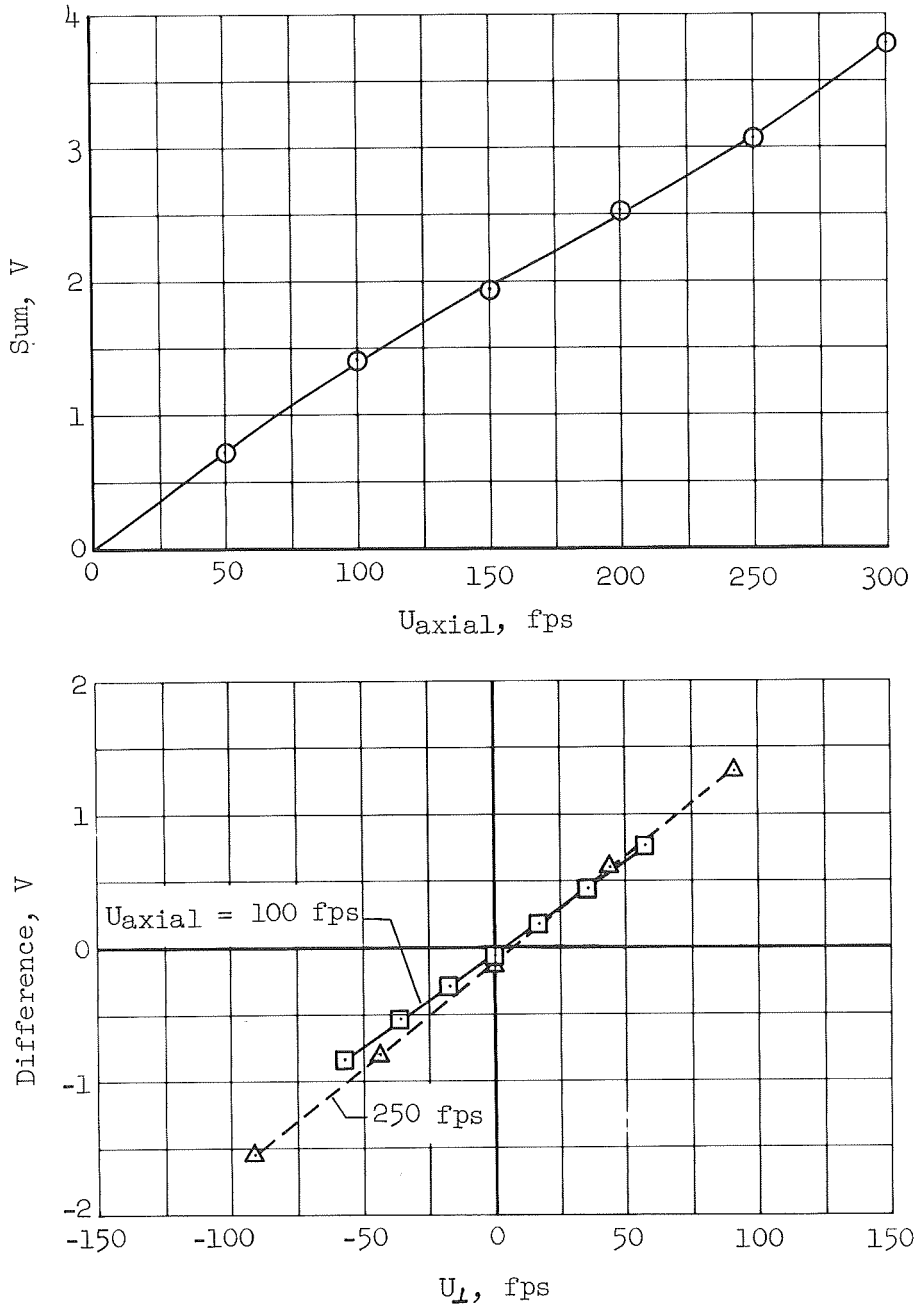

Figure 5.- Typical static calibrations of the hot wires.

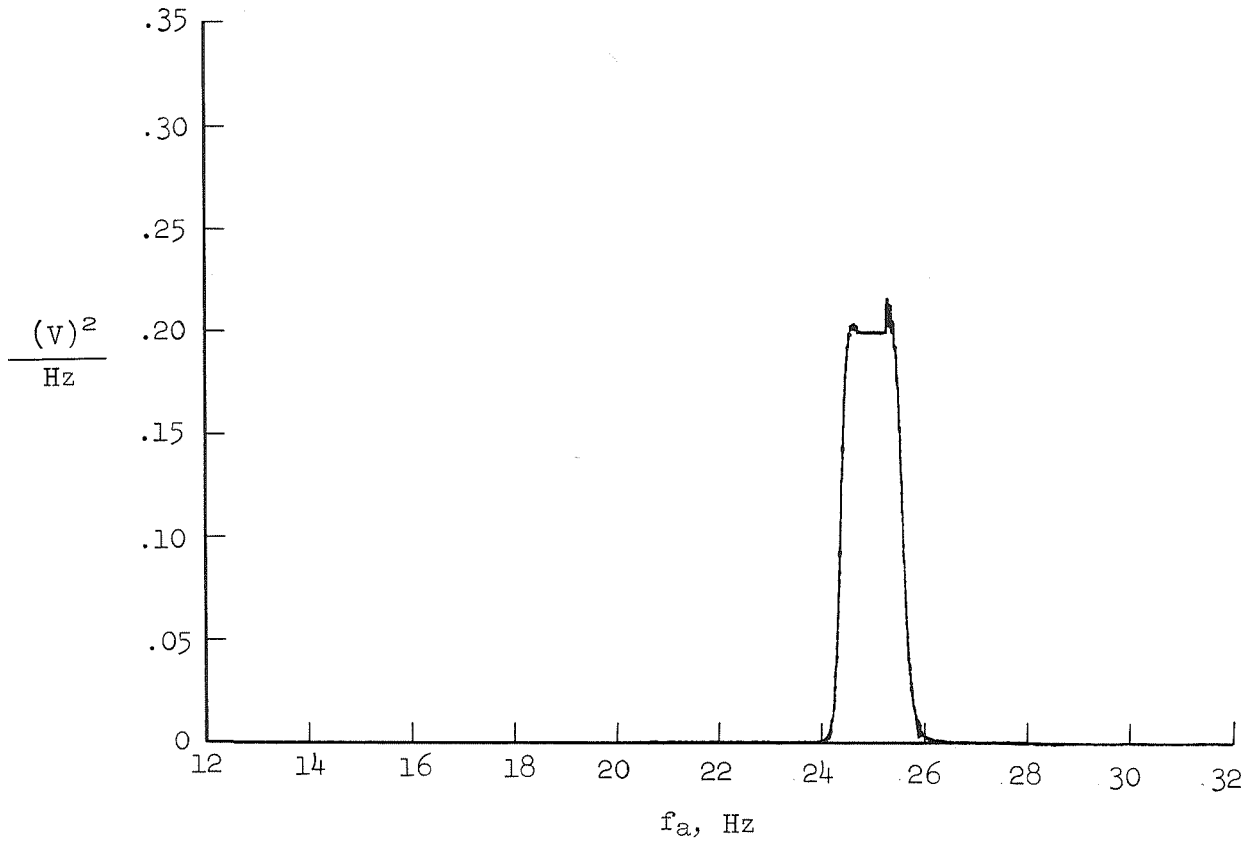

Figure 6.- Spectrum-analyzer output for 25-Hz calibration signal.

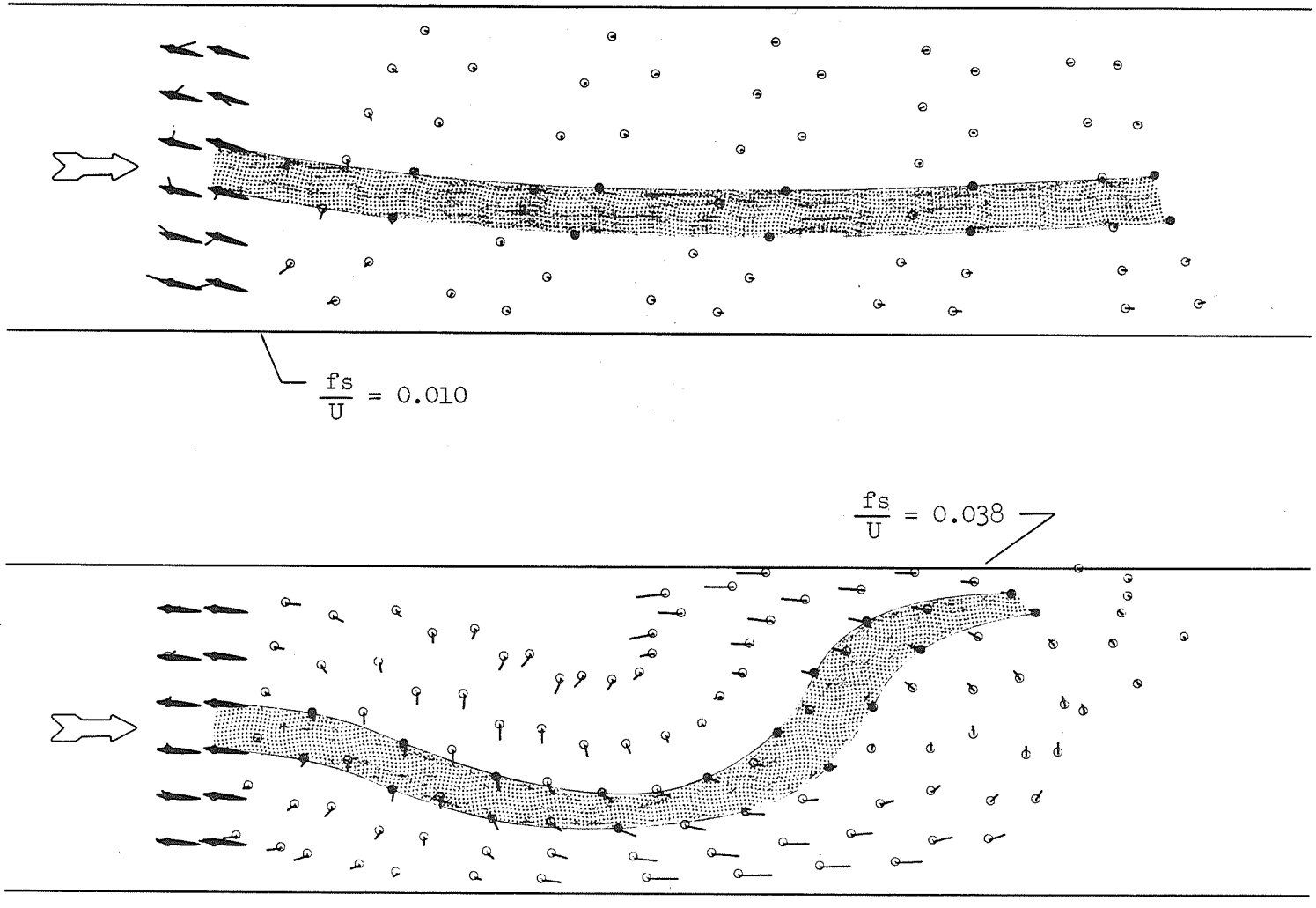

Figure 7.- Computed positions and velocities of low-strength point vortices shed from vanes in lateral-gust configuration B.

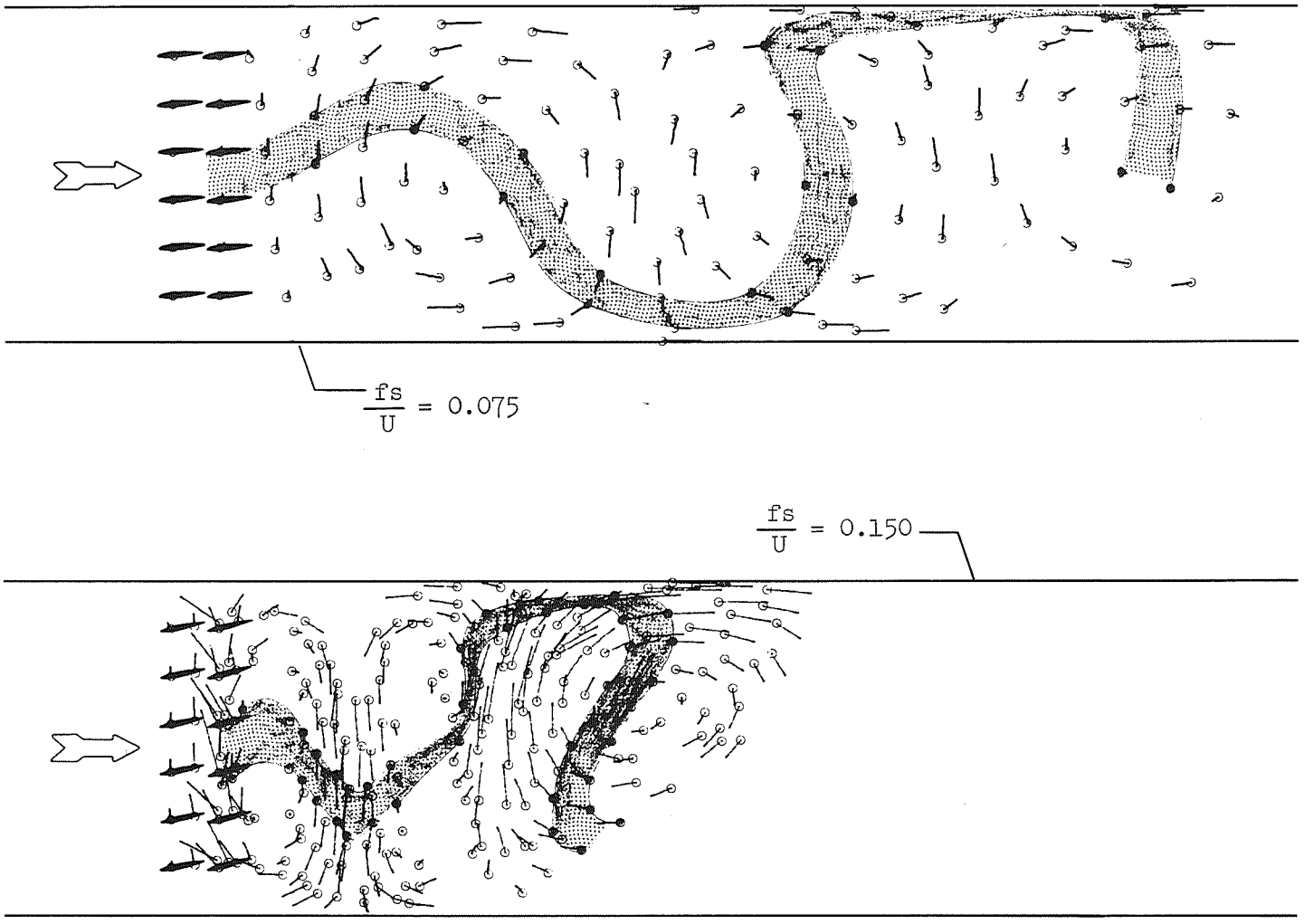

Figure 8.- Computed positions and velocities of high-strength point vortices shed from vanes in lateral-gust configuration B.

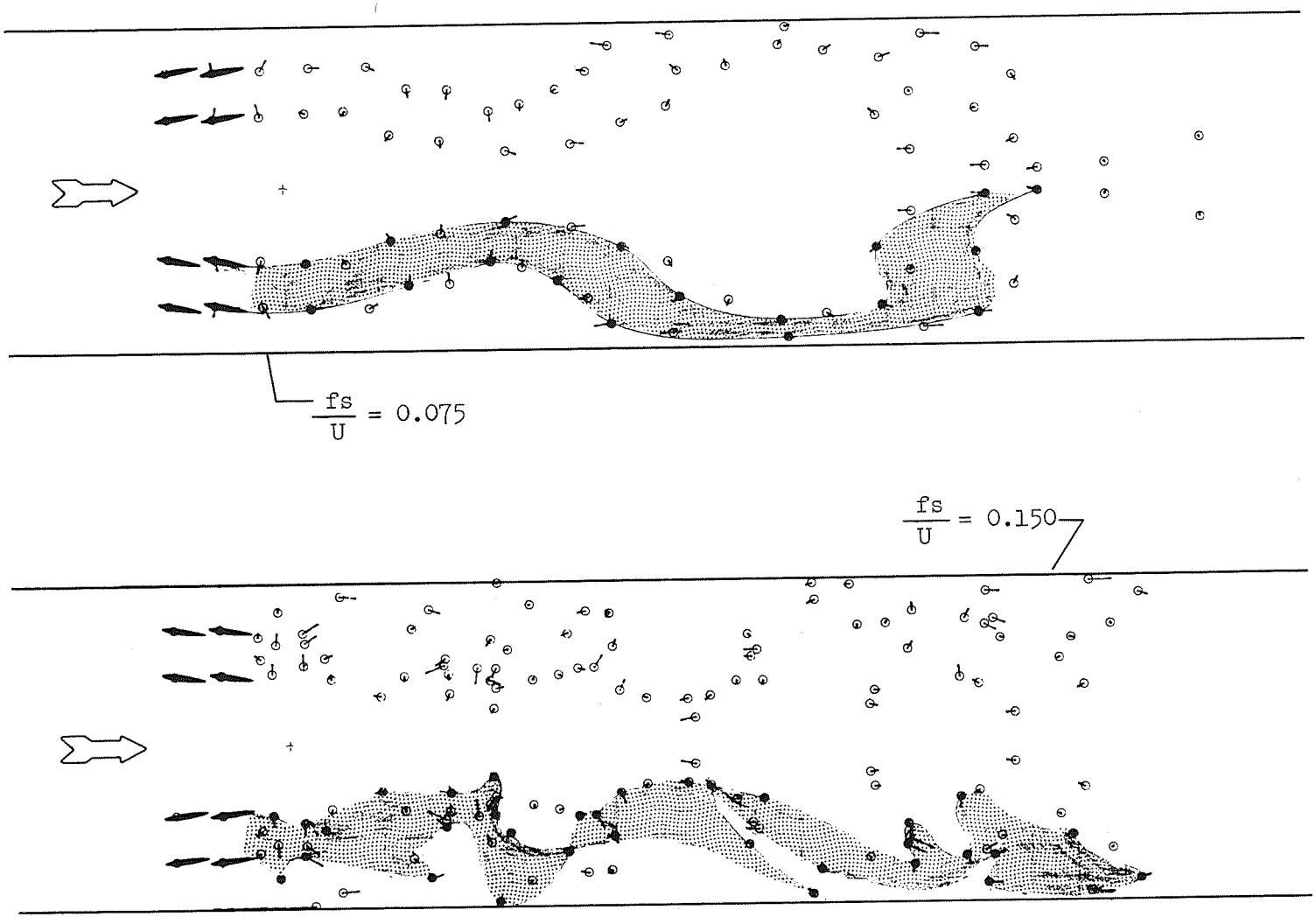

Figure 9.- Computed positions and velocities of point vortices shed from vanes in longitudinal-gust configuration J.

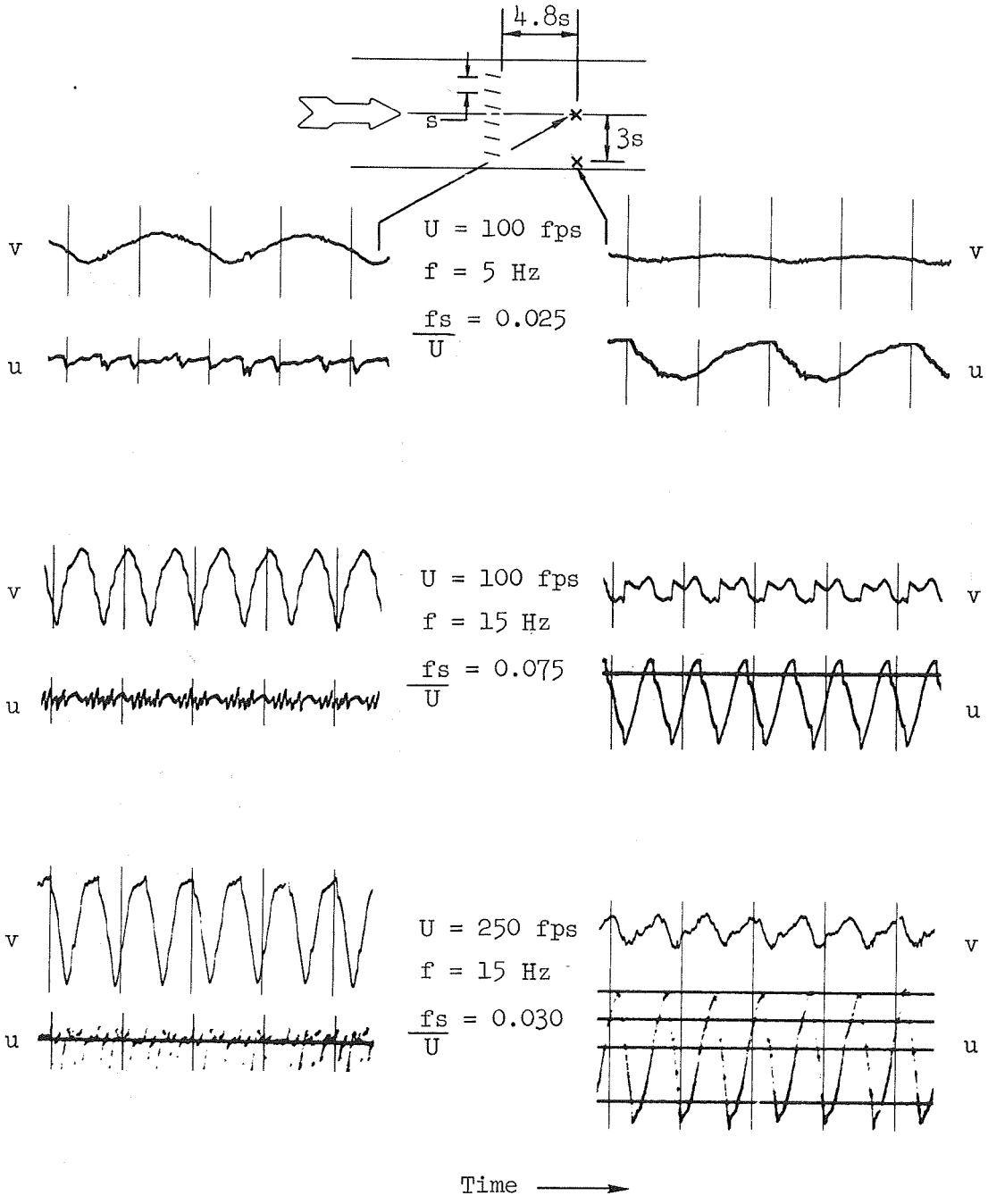

Figure 10.- Typical velocity time histories for lateral-gust configuration A; $\alpha_{max} = 15°$.

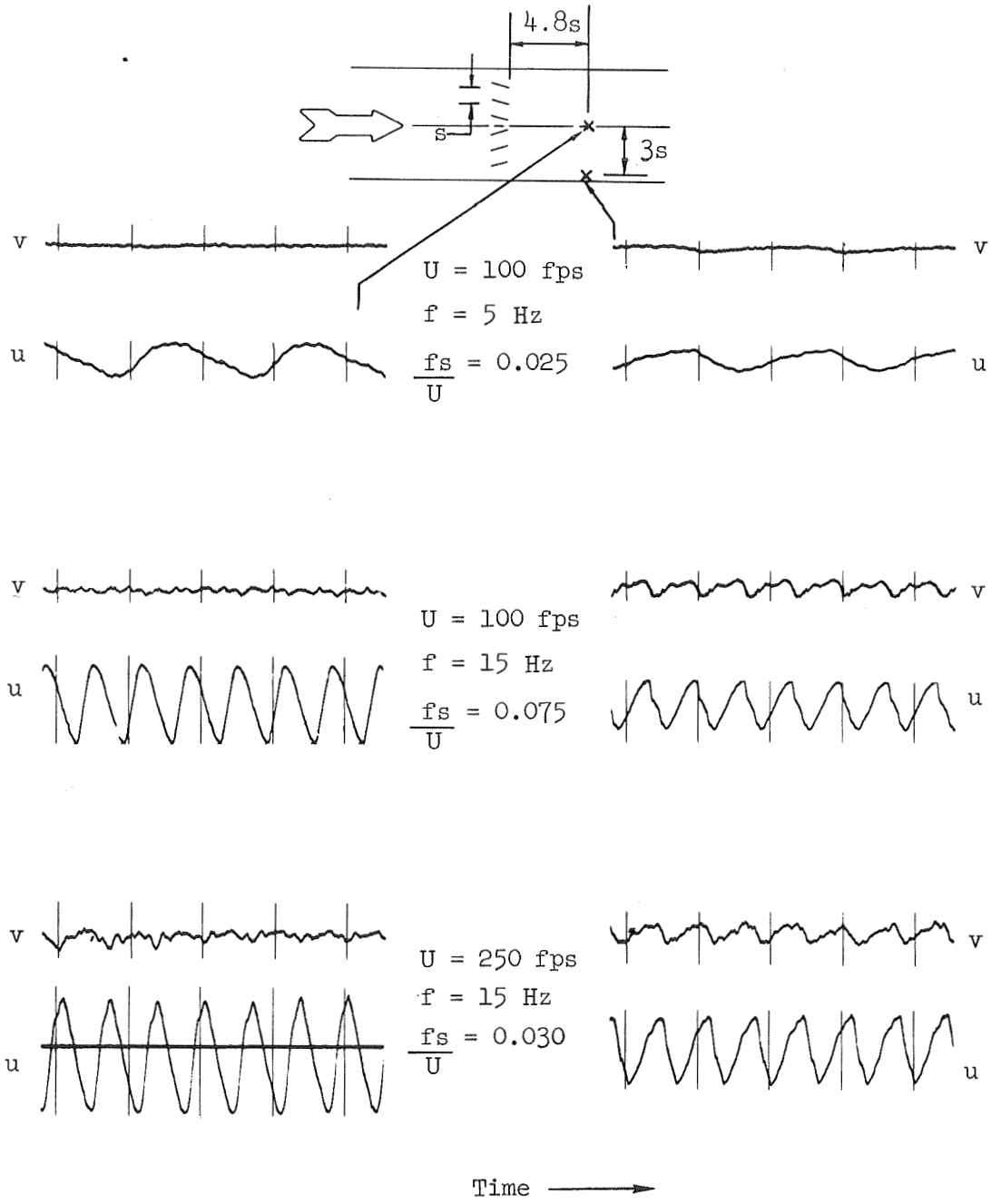

Figure 11.- Typical velocity time histories for longitudinal-gust configuration D; $\alpha_{max} \cong 12^{\circ}$.

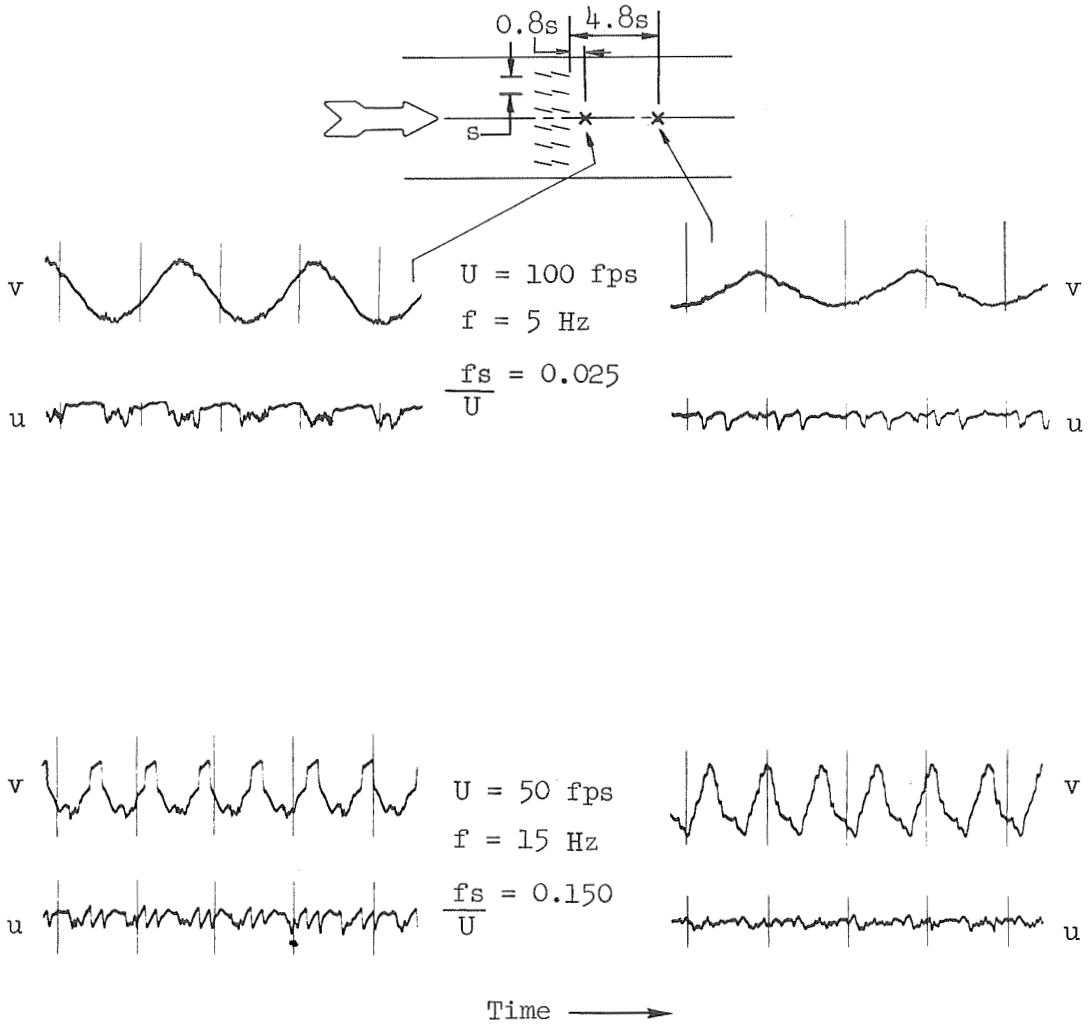

Figure 12.- Typical velocity time histories for lateral-gust configuration B; $\alpha_{max} \cong 13.50°$.

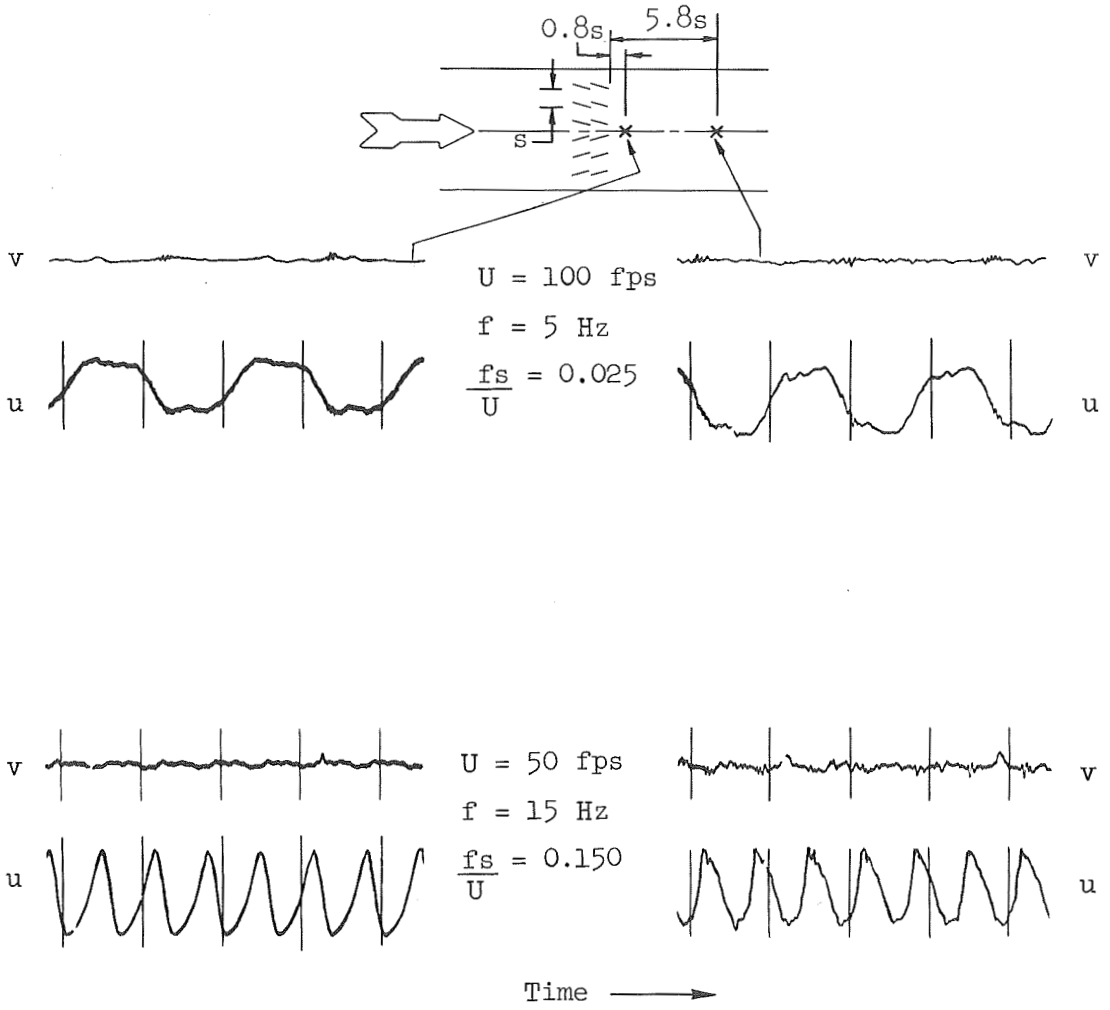

Figure 13.- Typical velocity time histories for longitudinal-gust configuration E; $\alpha_{max} \cong 12.50°$.

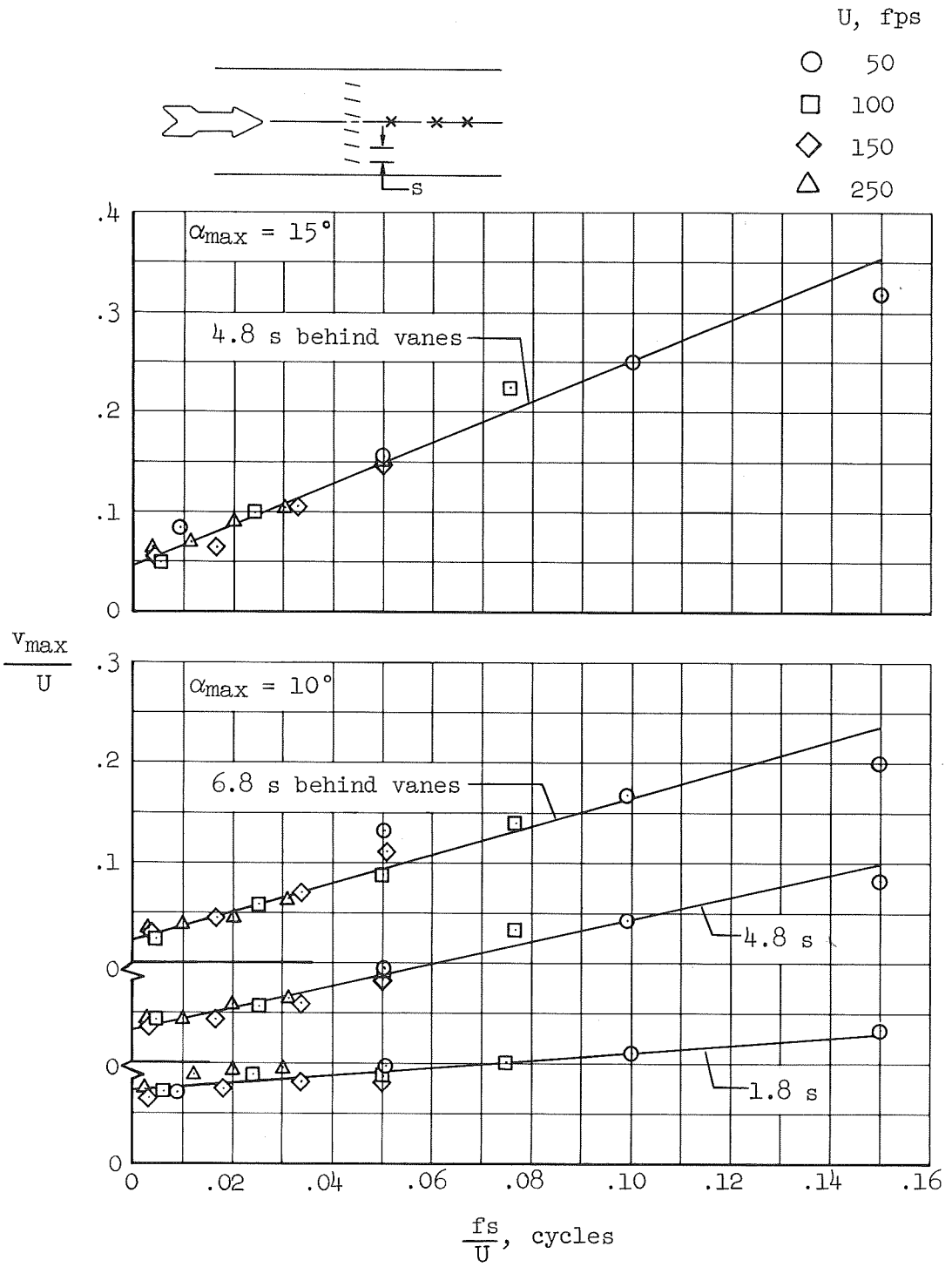

Figure 14.- Lateral-gust amplitudes on the channel centerline behind lateral-gust configuration A.

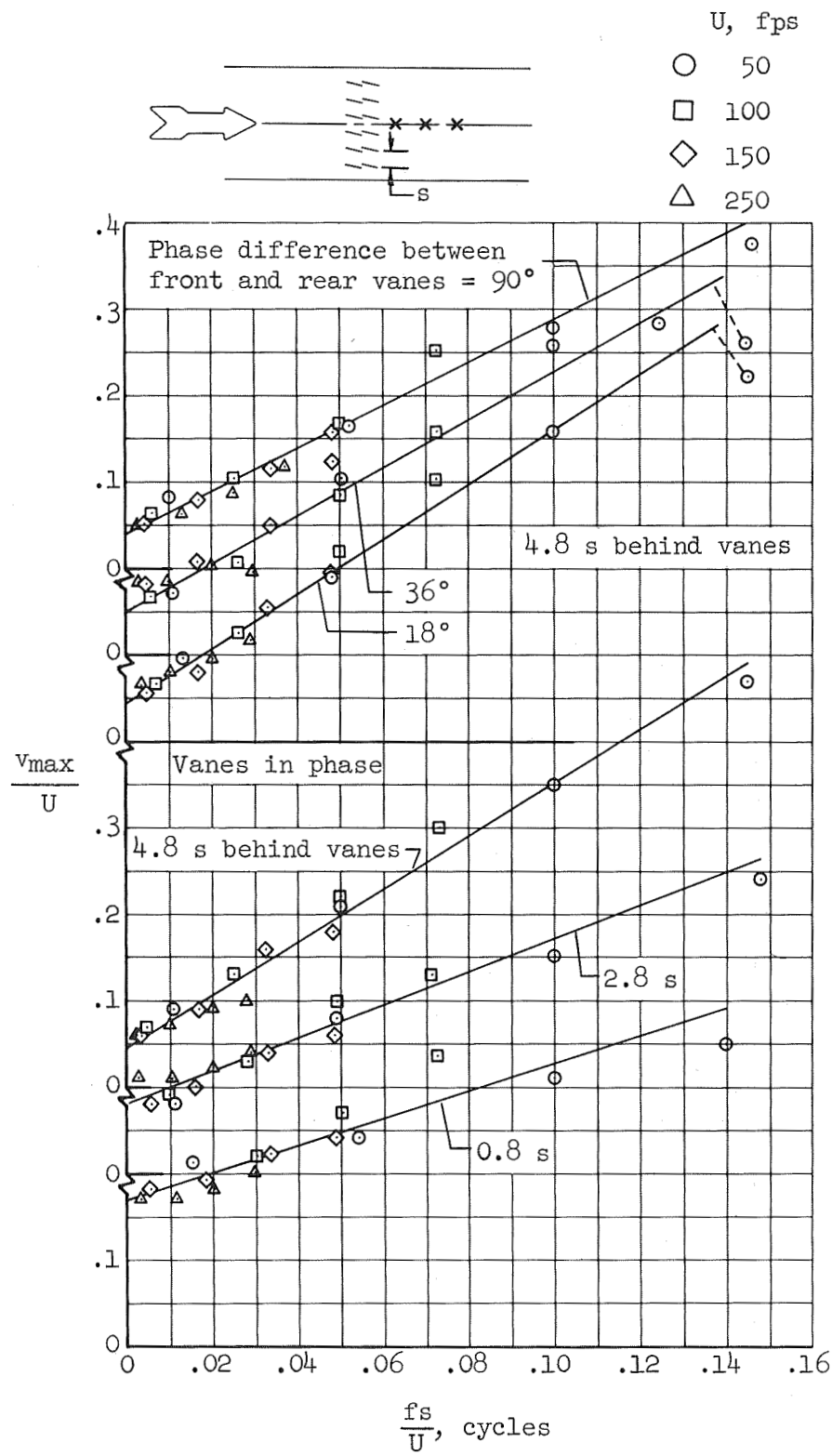

Figure 15.- Lateral-gust amplitudes on the channel centerline behind lateral-gust configuration B; $\alpha_{max} \cong 13.50°$.

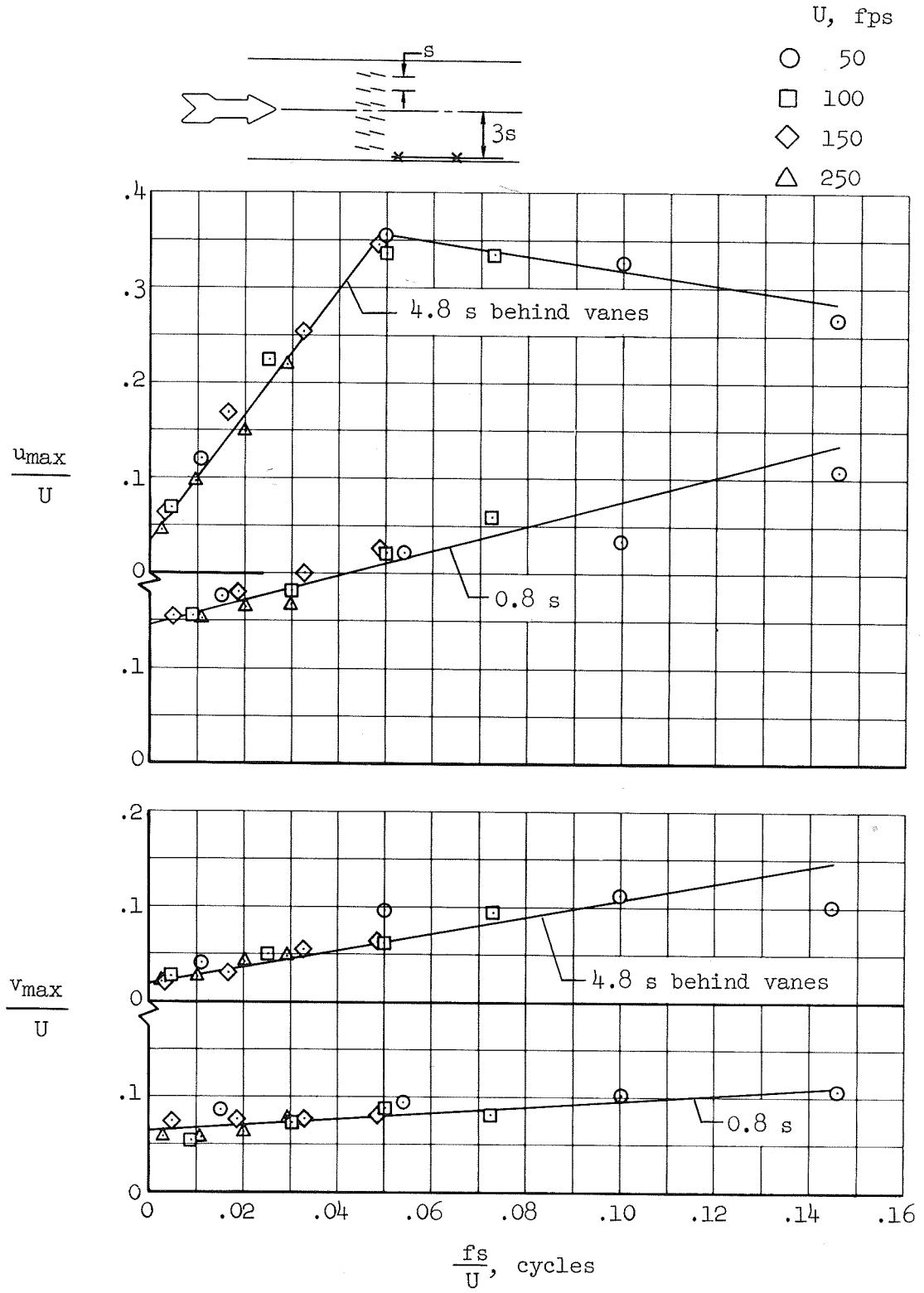

Figure 16.- Gust amplitudes near the channel wall behind lateral-gust configuration B; $\alpha_{max} \cong 13.50°$.

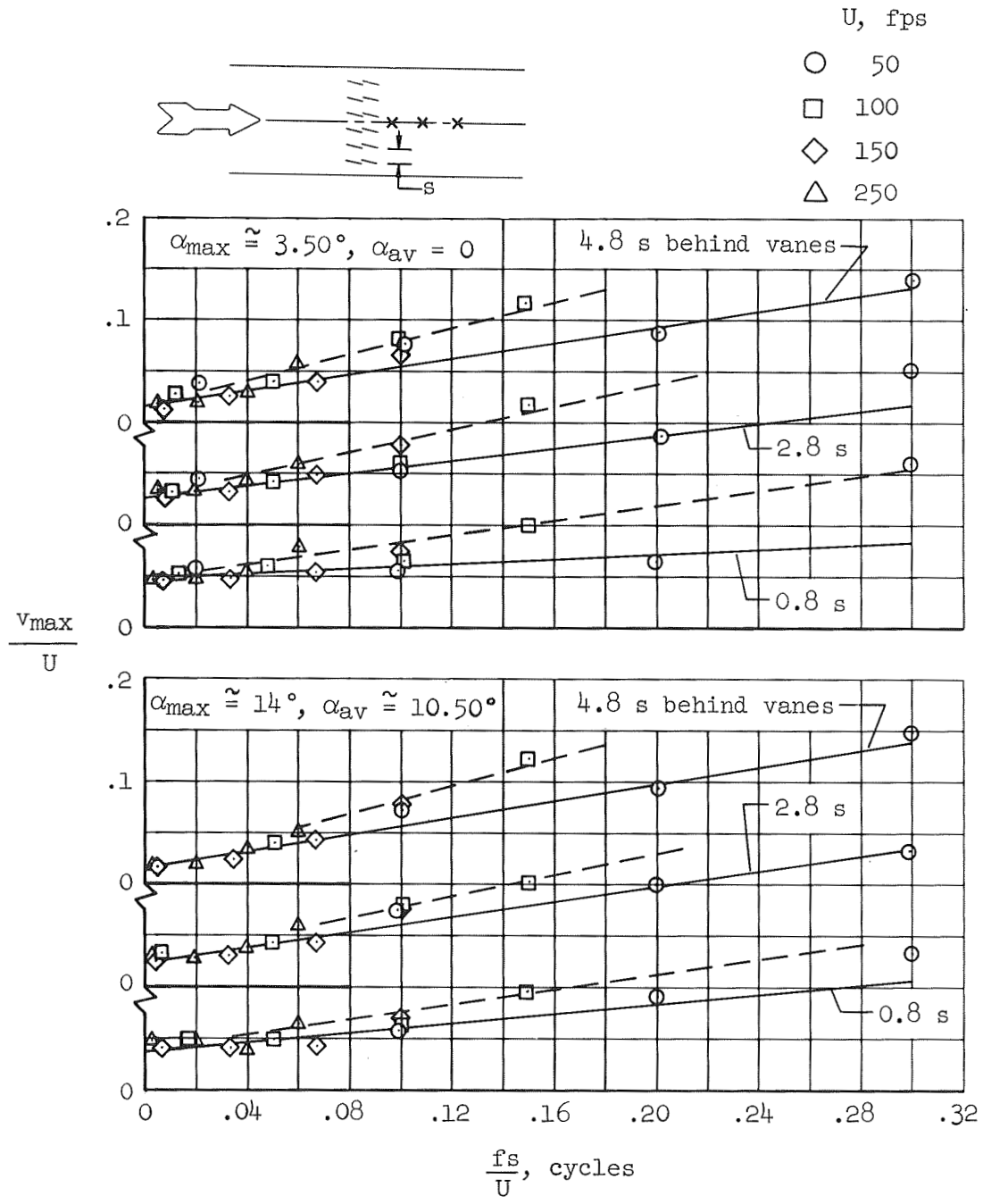

Figure 17.- Lateral-gust amplitudes on the channel centerline behind lateral-gust configuration B oscillating at small amplitudes.

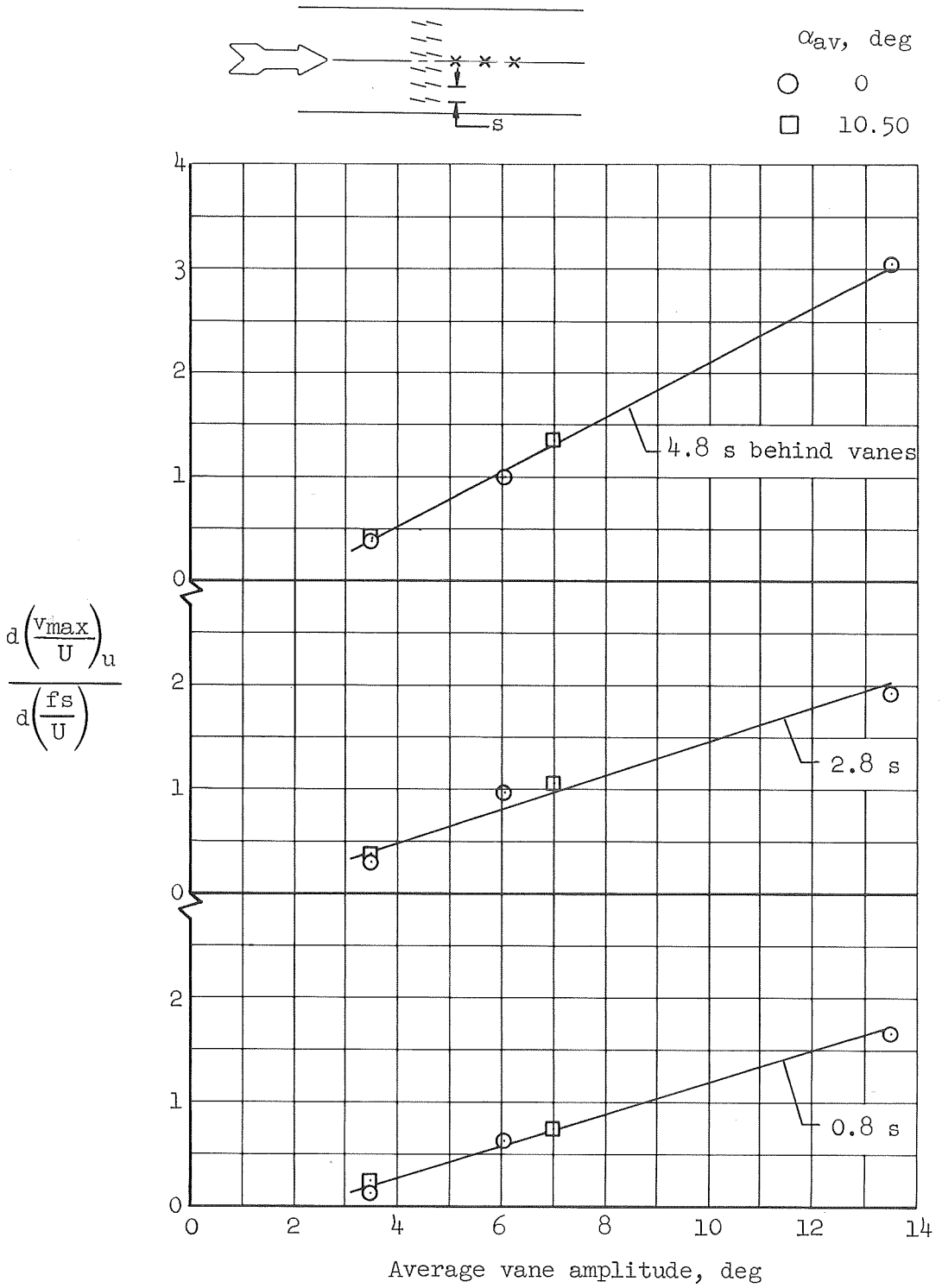

Figure 18.- The variation of the uncorrected gust-frequency slope with actual vane-oscillation amplitude on the channel center-line behind lateral-gust configuration B.

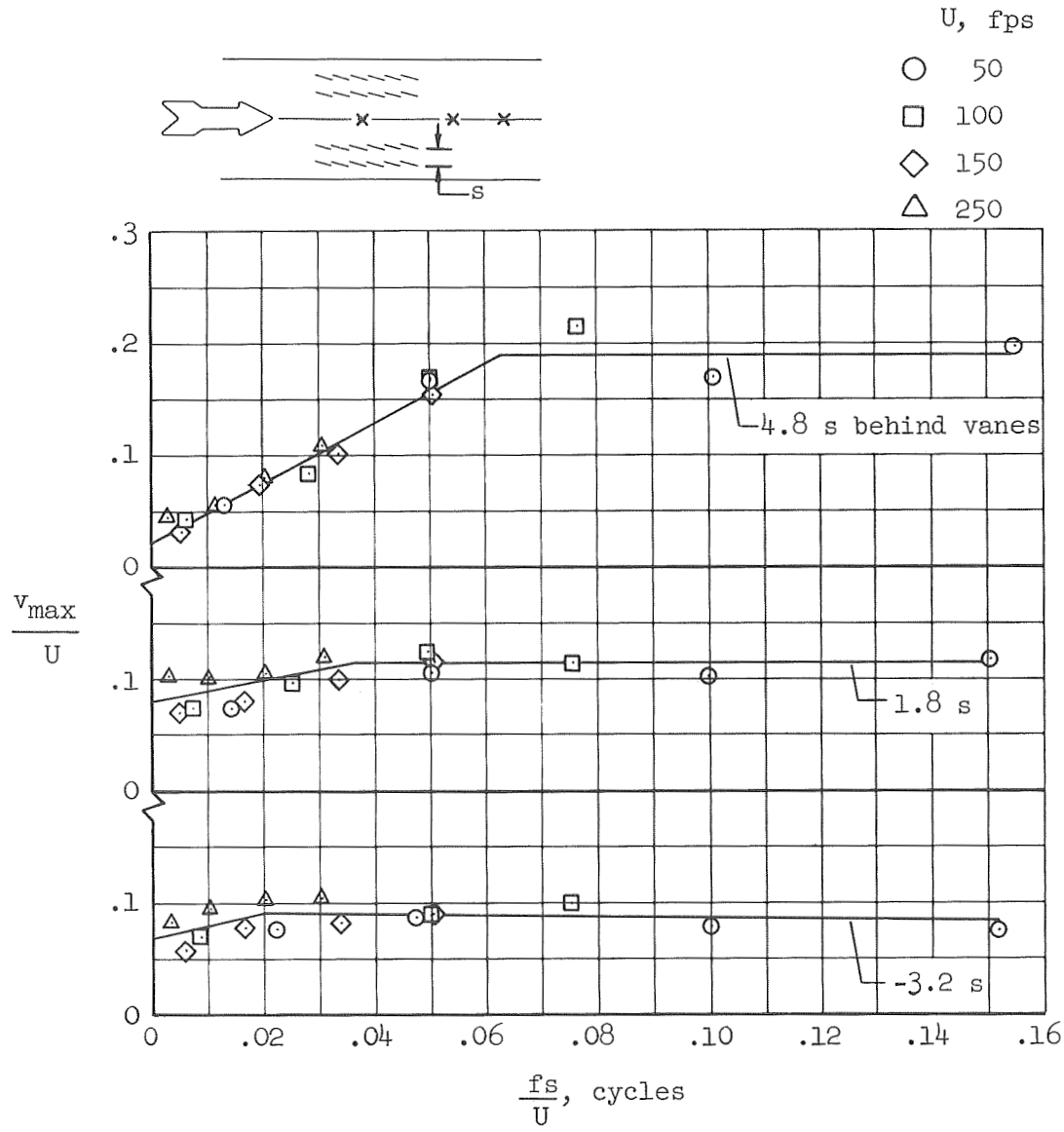

Figure 19.- Lateral-gust amplitudes on the channel centerline behind lateral-gust configuration C; α_{max} = 12°.

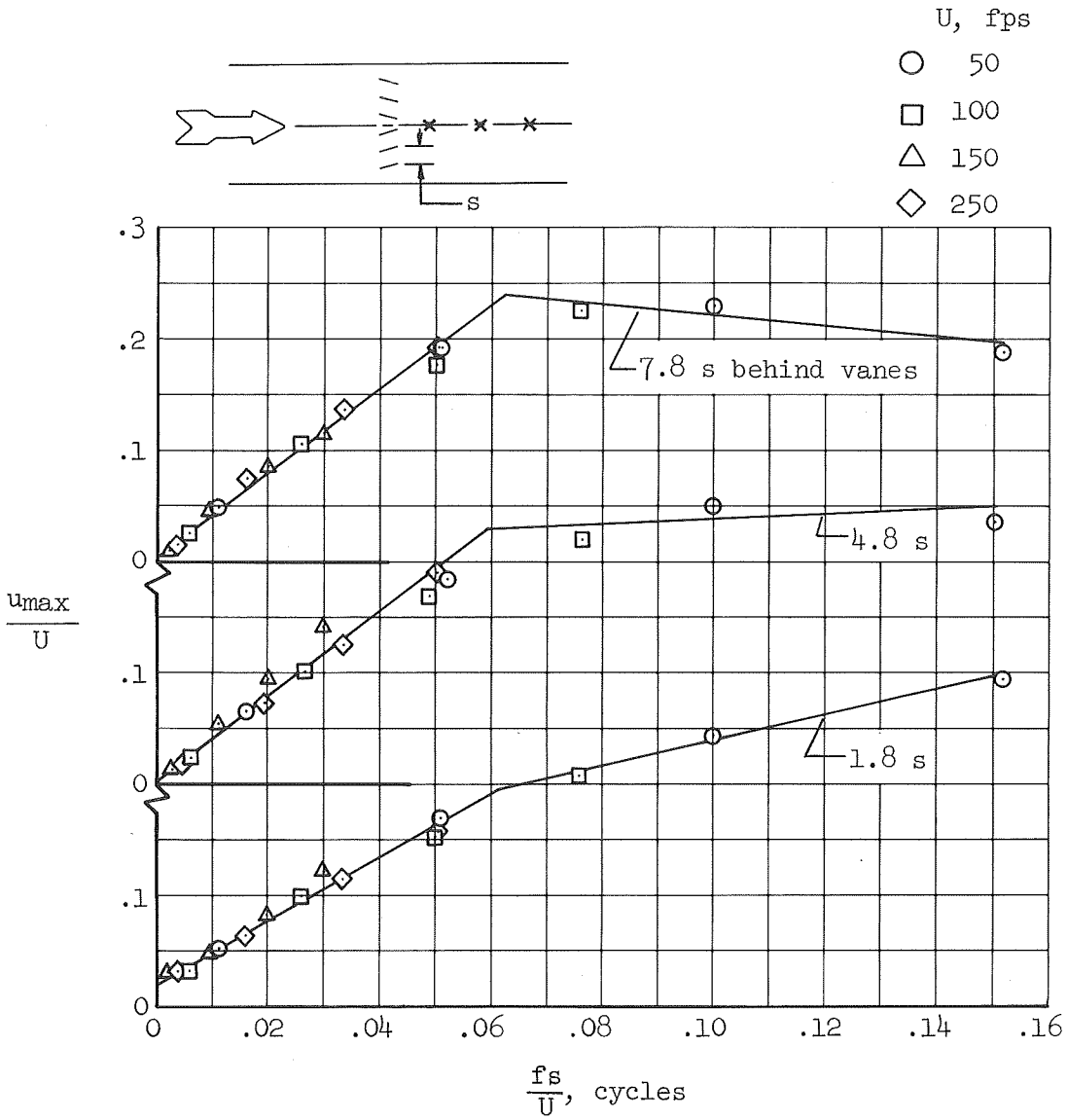

Figure 20.- Longitudinal-gust amplitudes on the channel centerline behind longitudinal-gust configuration D; α_{max} = 12°.

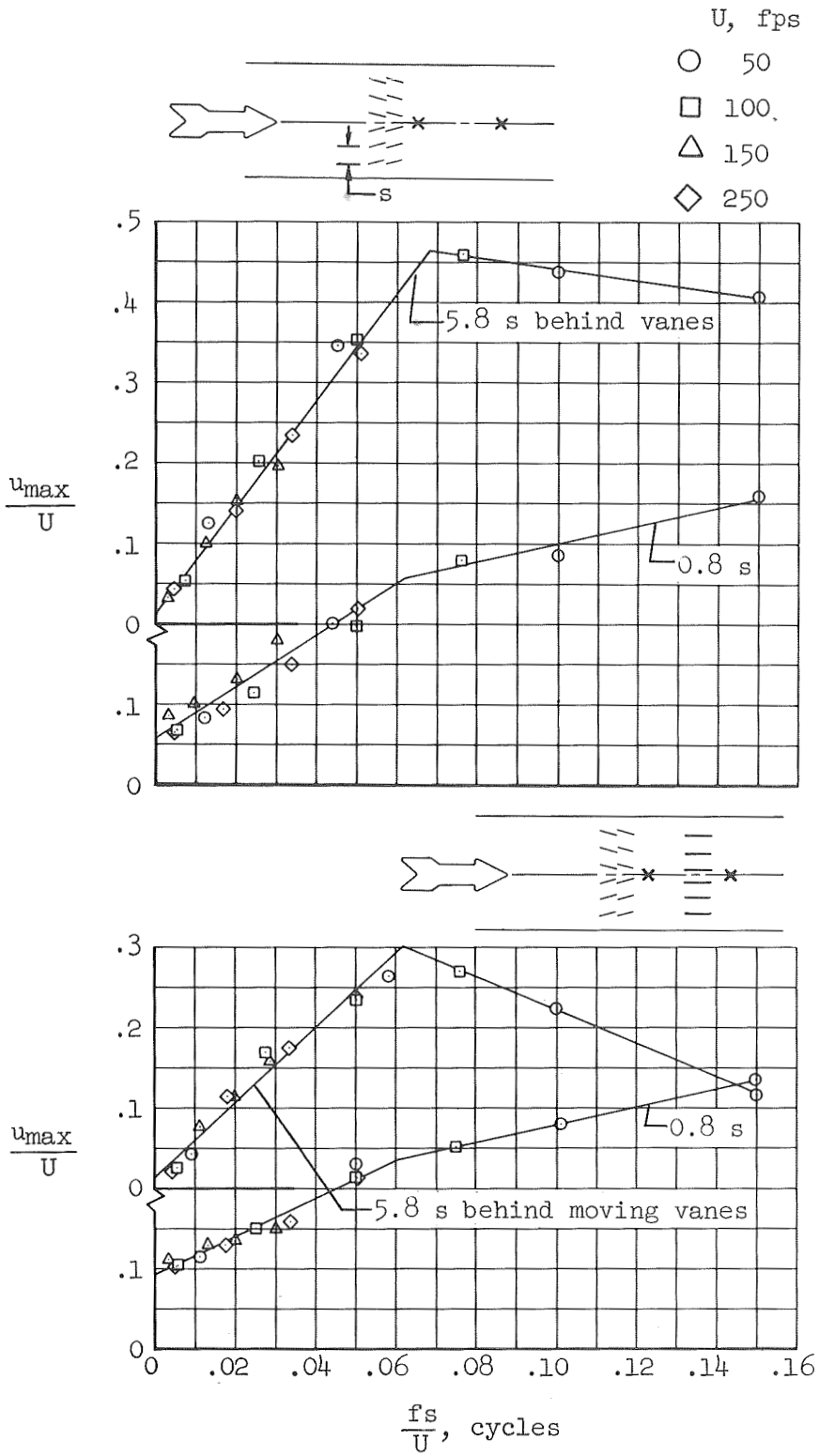

Figure 21.- Longitudinal-gust amplitudes on the channel centerline behind longitudinal-gust configurations E and F; $\alpha_{max} \cong 12.50°$.

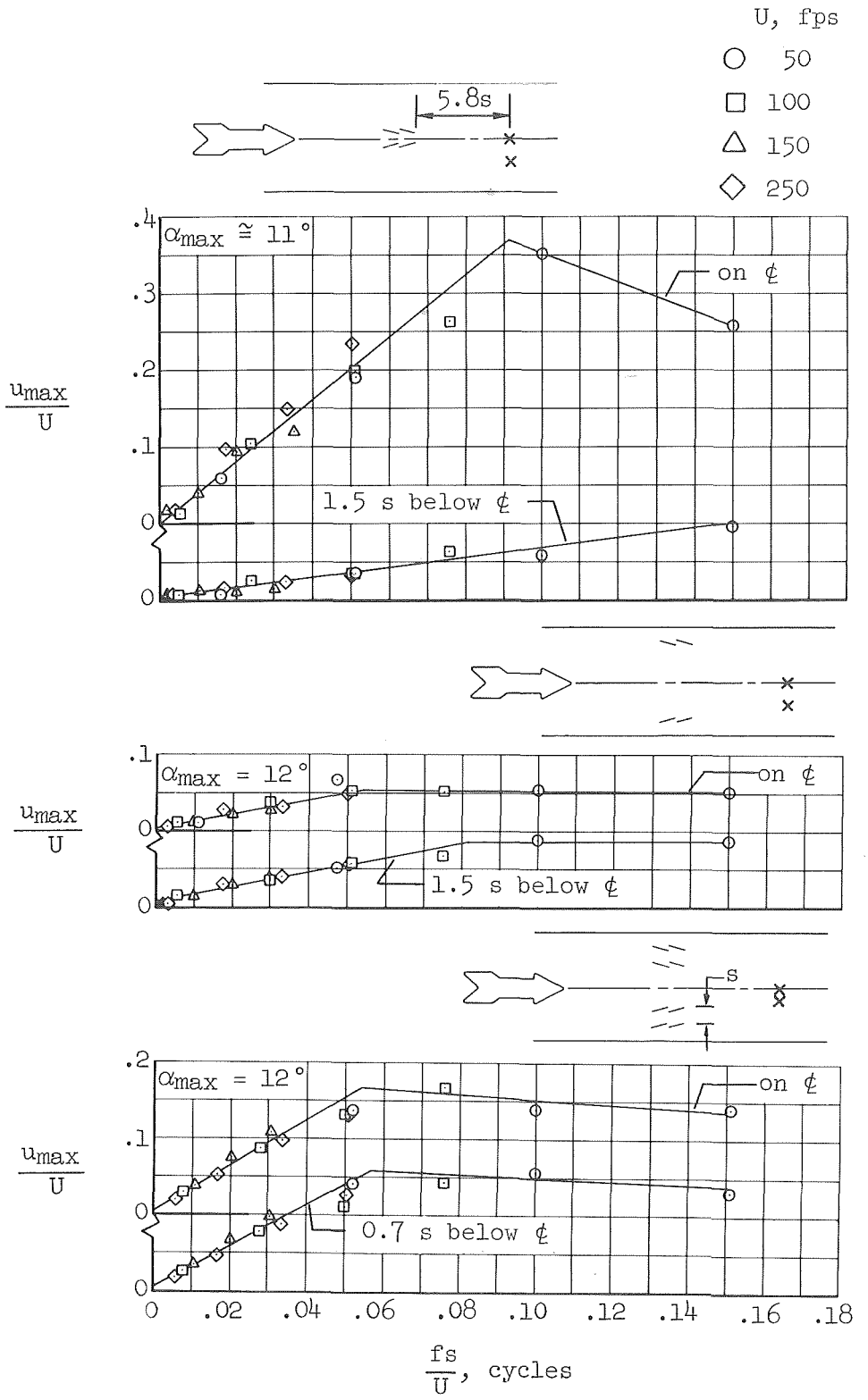

Figure 22.- Longitudinal-gust amplitudes behind longitudinal-gust configurations G, H, and J.

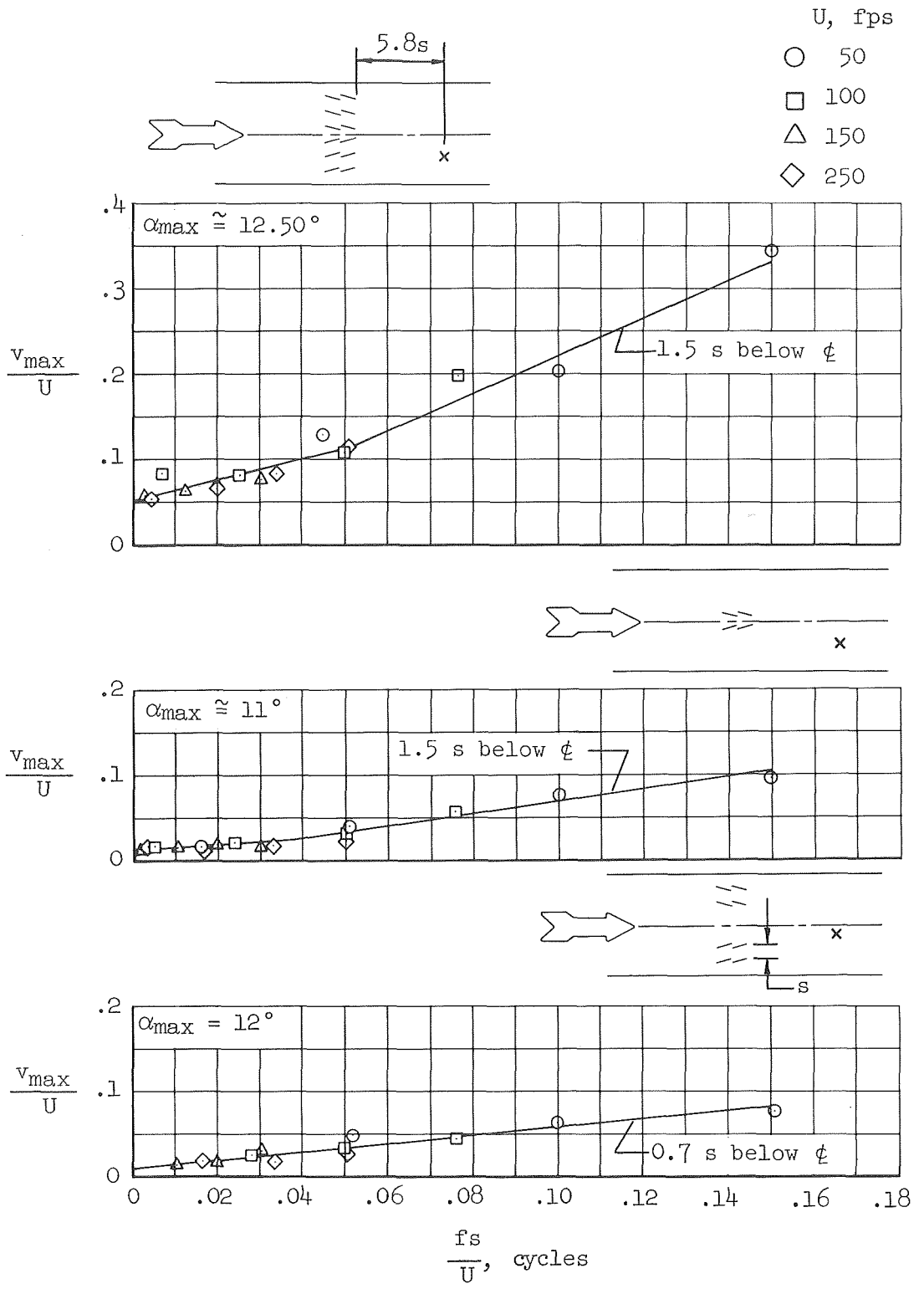

Figure 23.- Lateral-gust amplitudes behind longitudinal-gust configurations E, G, and J.

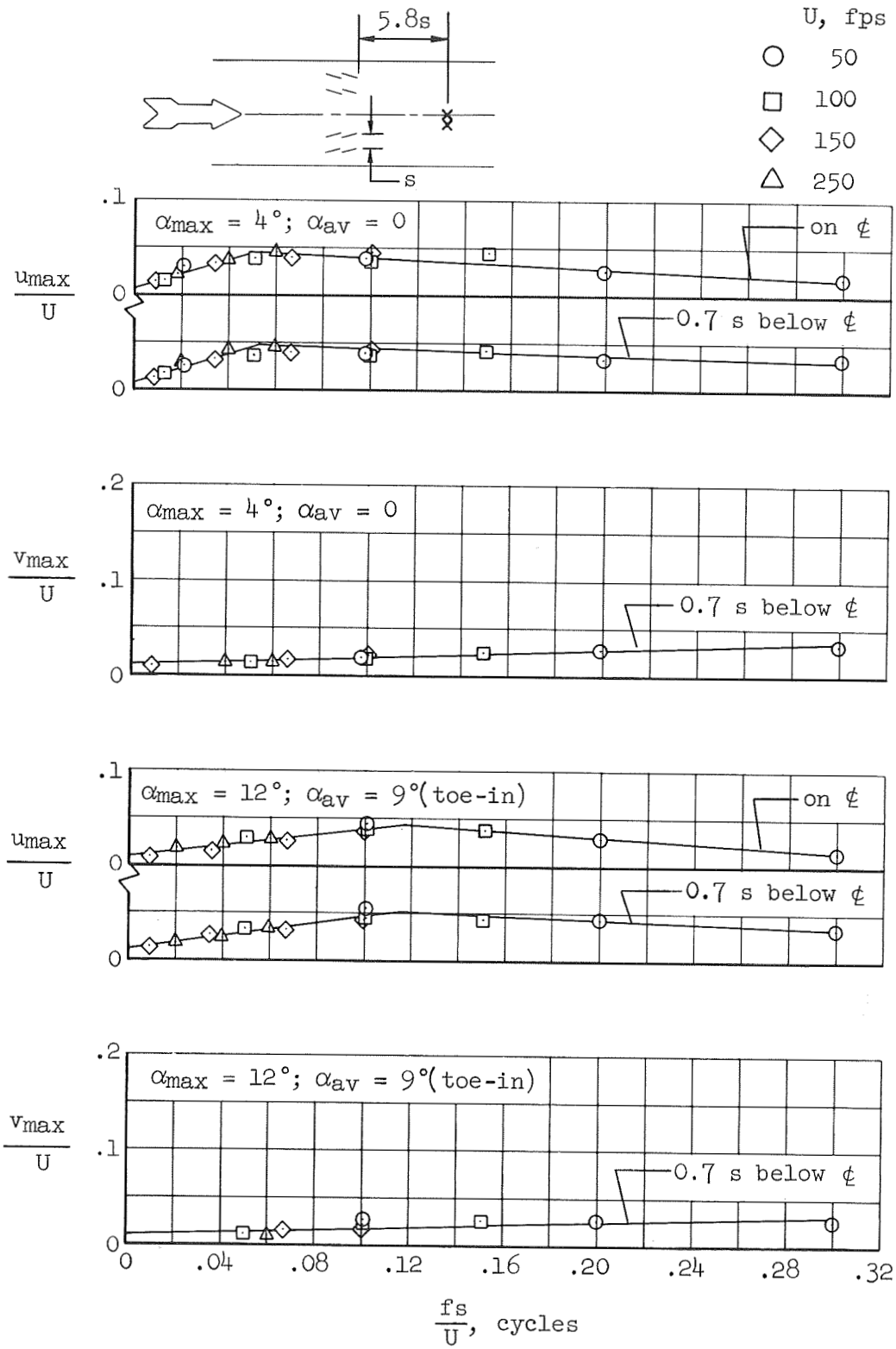

Figure 24.- Gust amplitudes behind longitudinal-gust configuration J oscillating at small amplitudes.

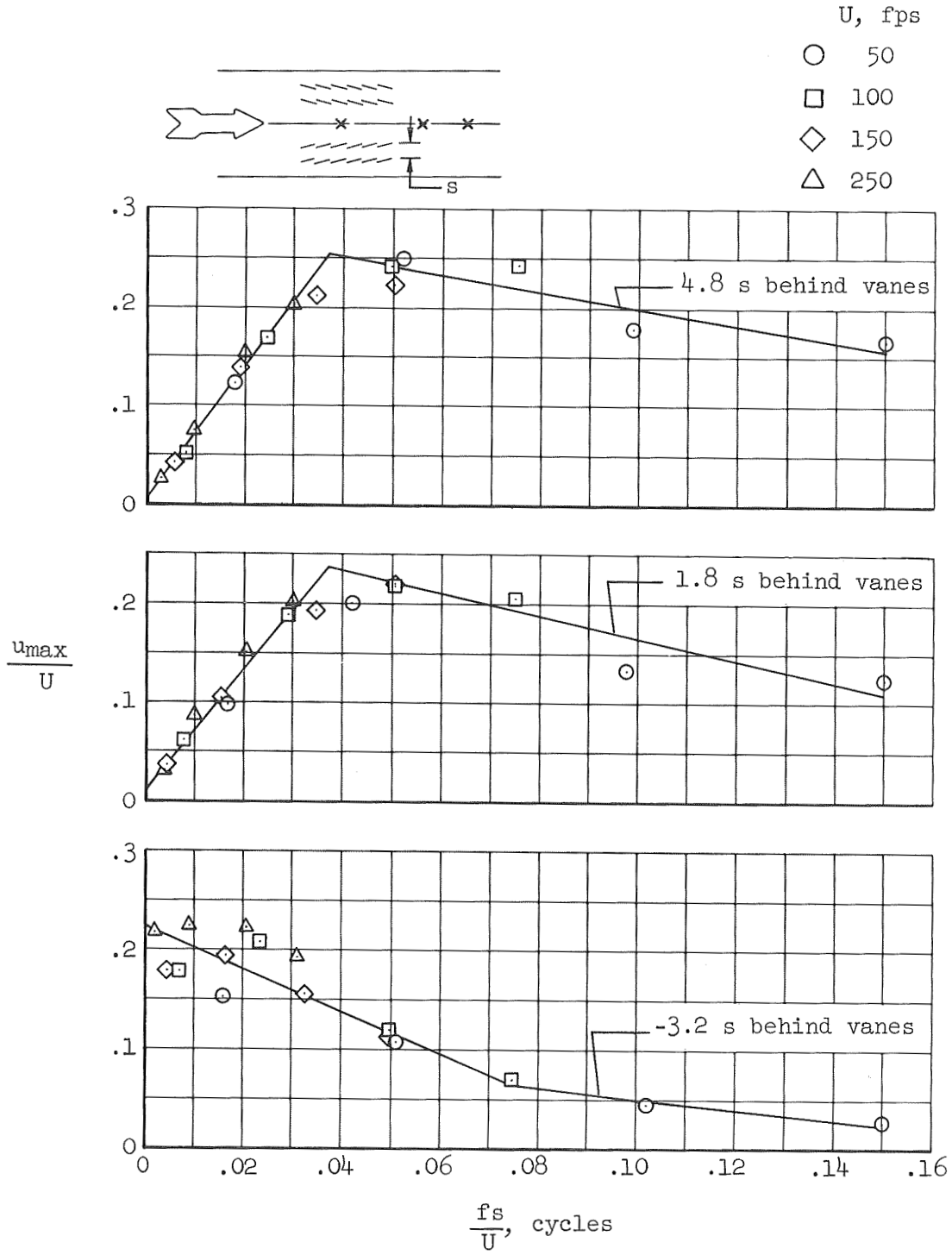

Figure 25.- Longitudinal-gust amplitudes on the channel centerline near longitudinal-gust configuration K; α_{max} = 12°.

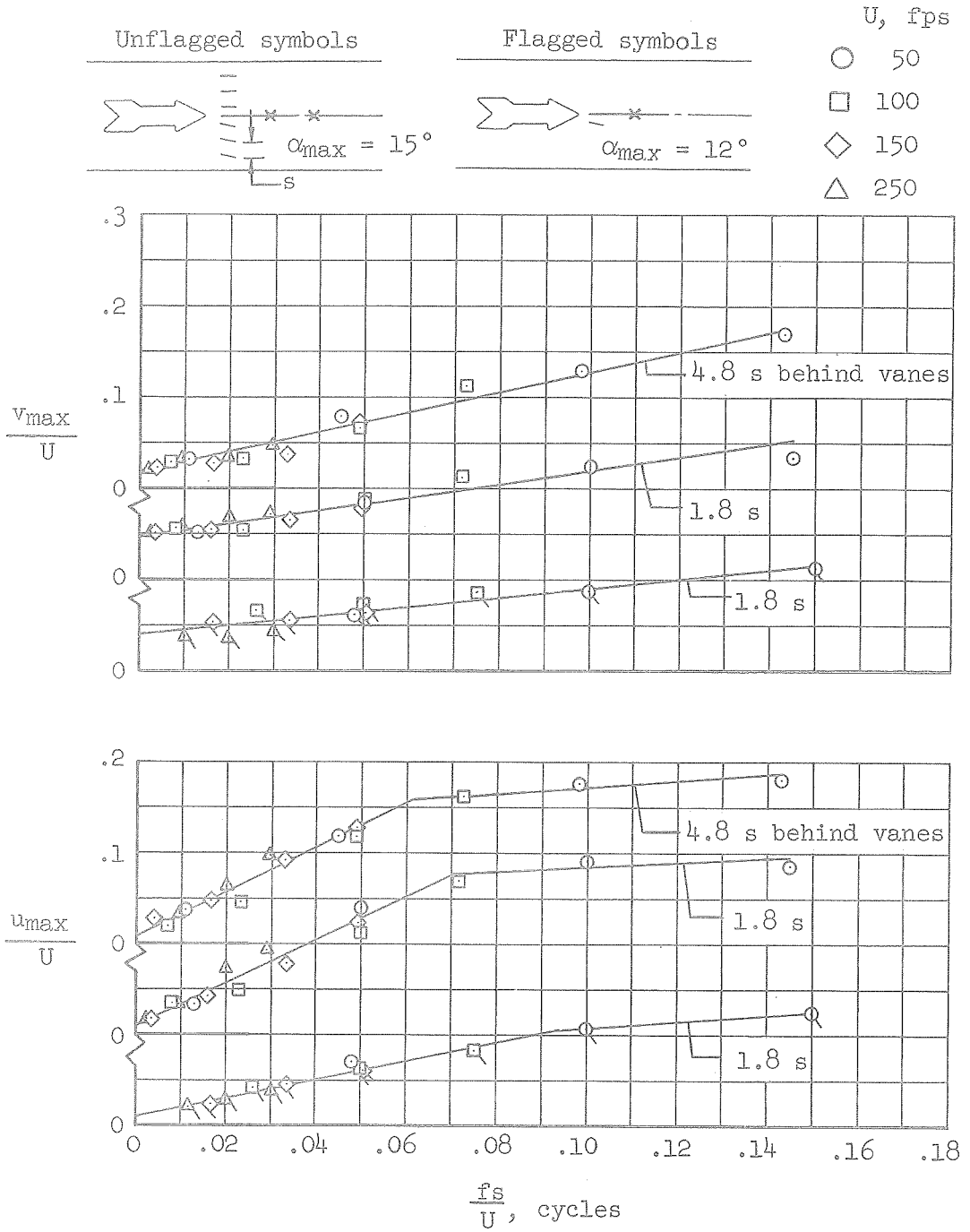

Figure 26.- Gust amplitudes on the channel centerline behind axisymmetric configurations L and M.

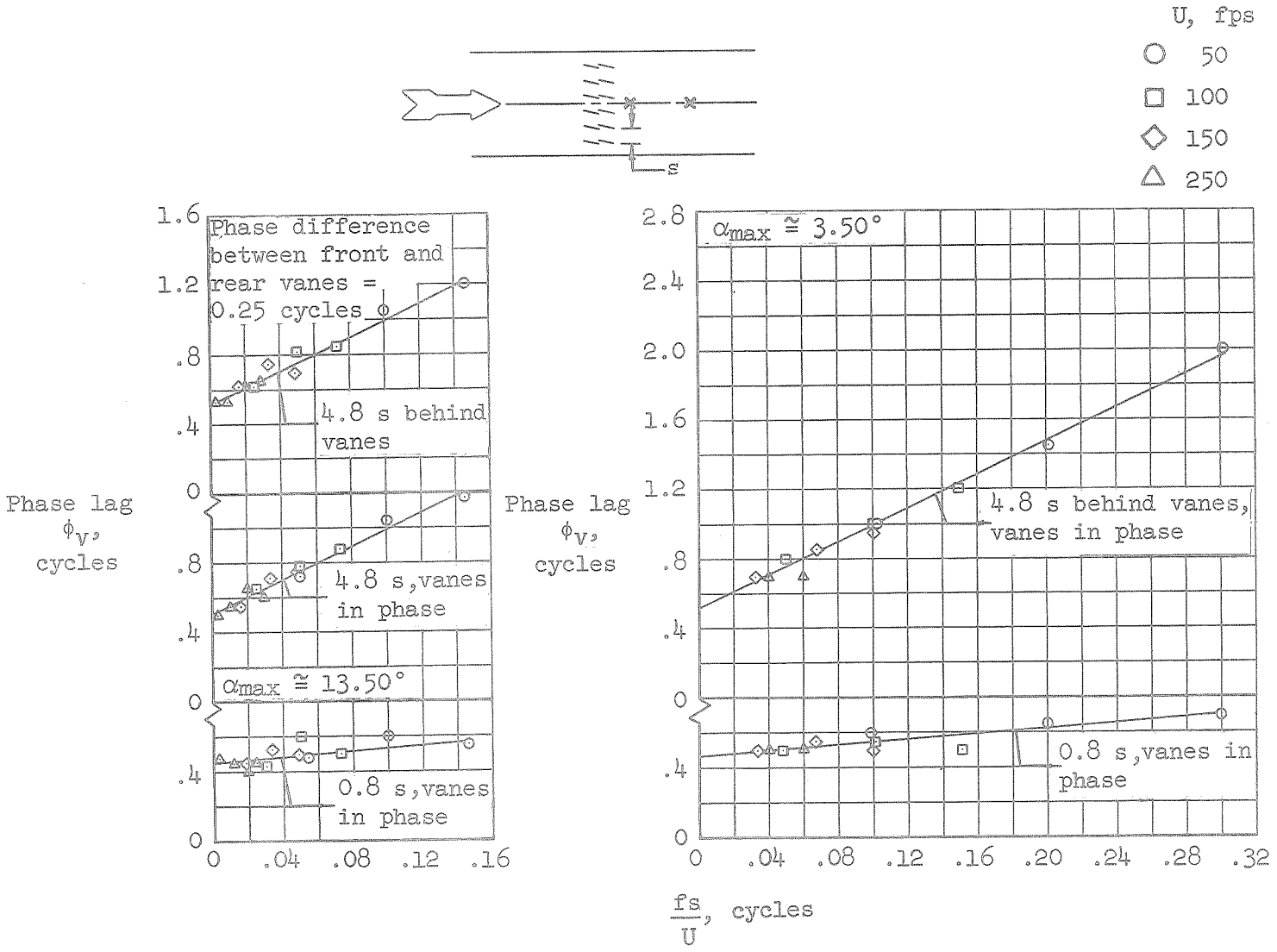

Figure 27.- Phase lag with respect to vane motion of lateral gusts on the channel centerline behind lateral-gust configuration B.

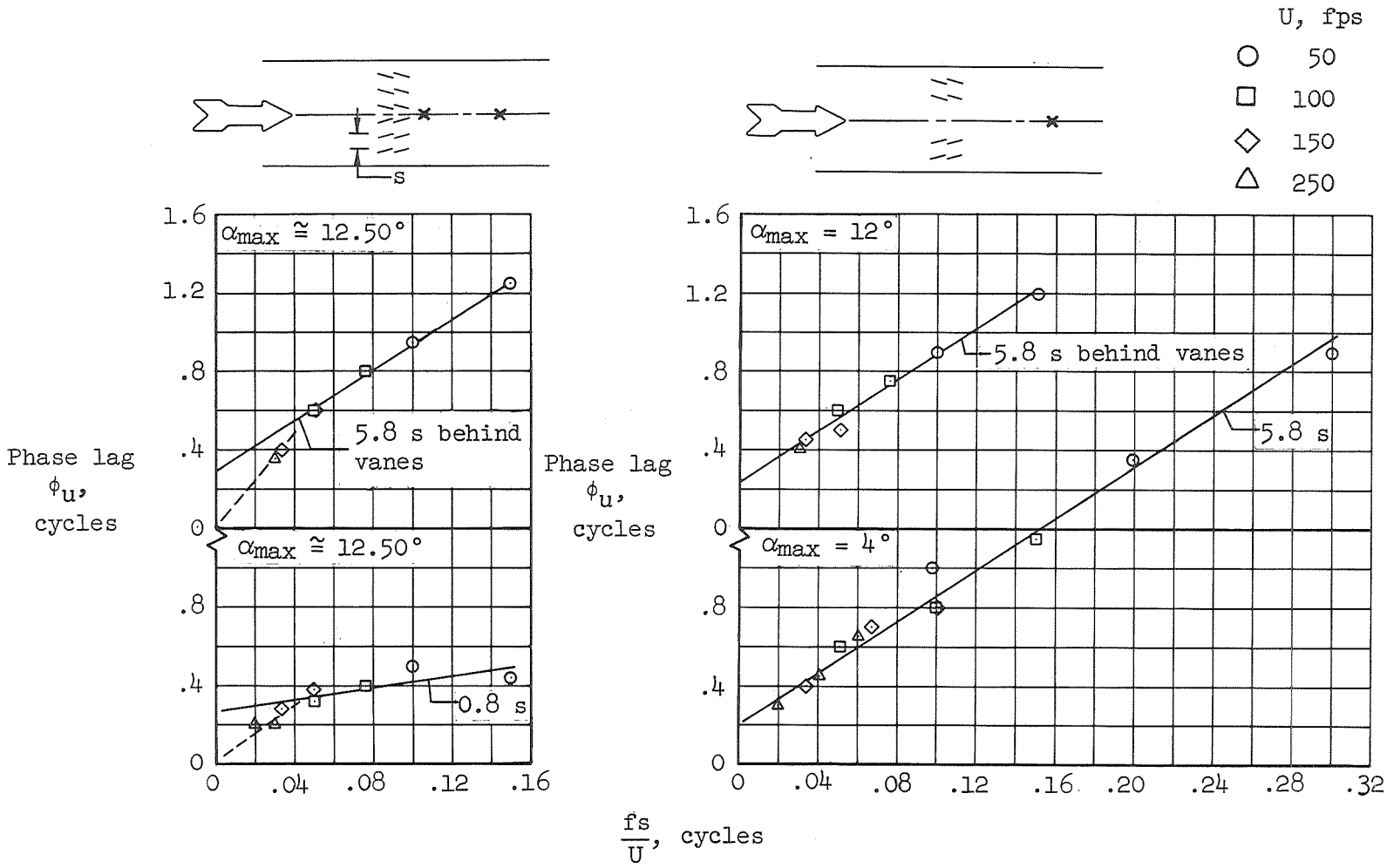

Figure 28.- Phase lag with respect to vane motion of longitudinal gusts on the channel centerline behind longitudinal gust configurations E and J.

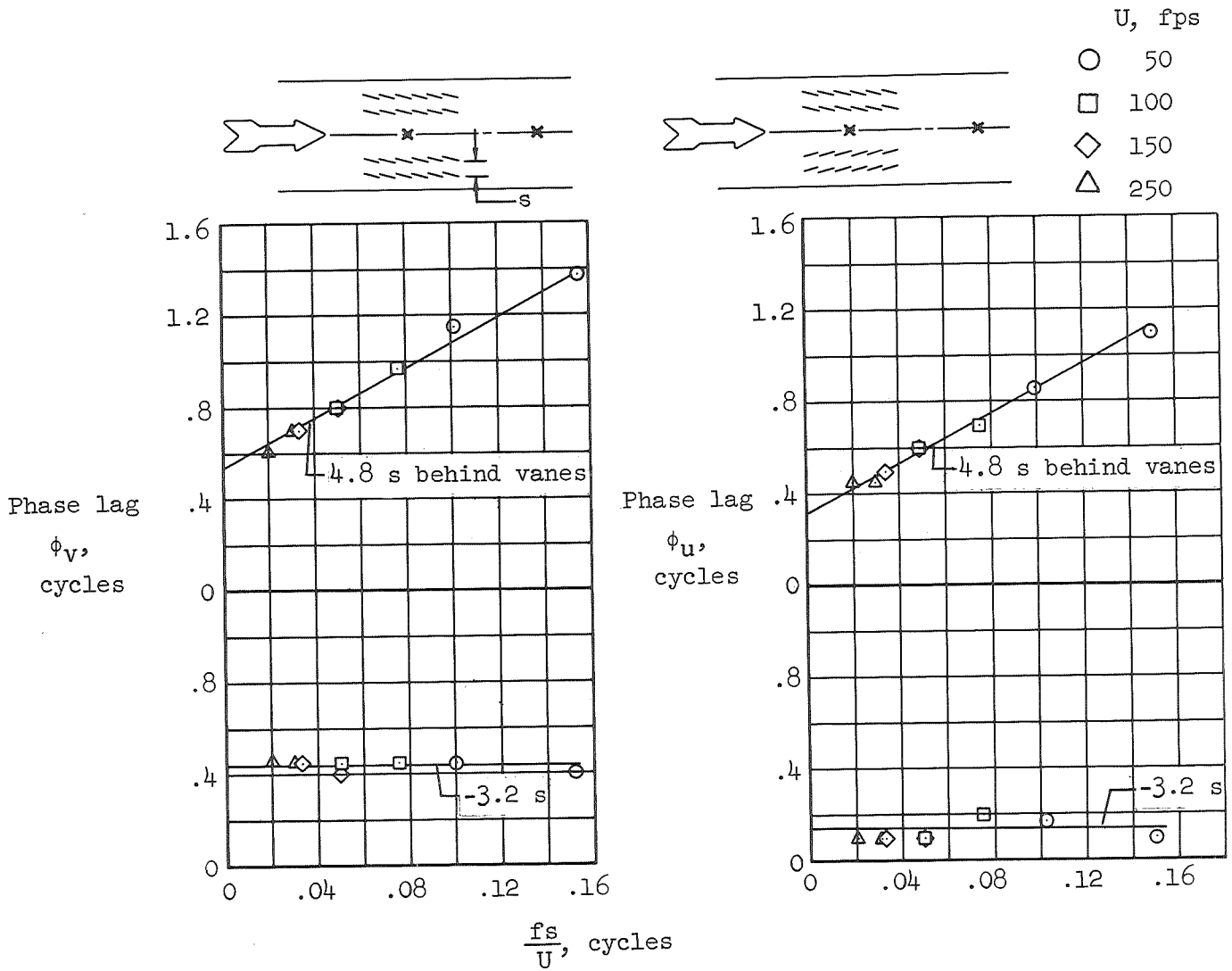

Figure 29.- Phase lag with respect to vane motion of gusts near vane configurations C and K; $\alpha_{max} = 12°$.

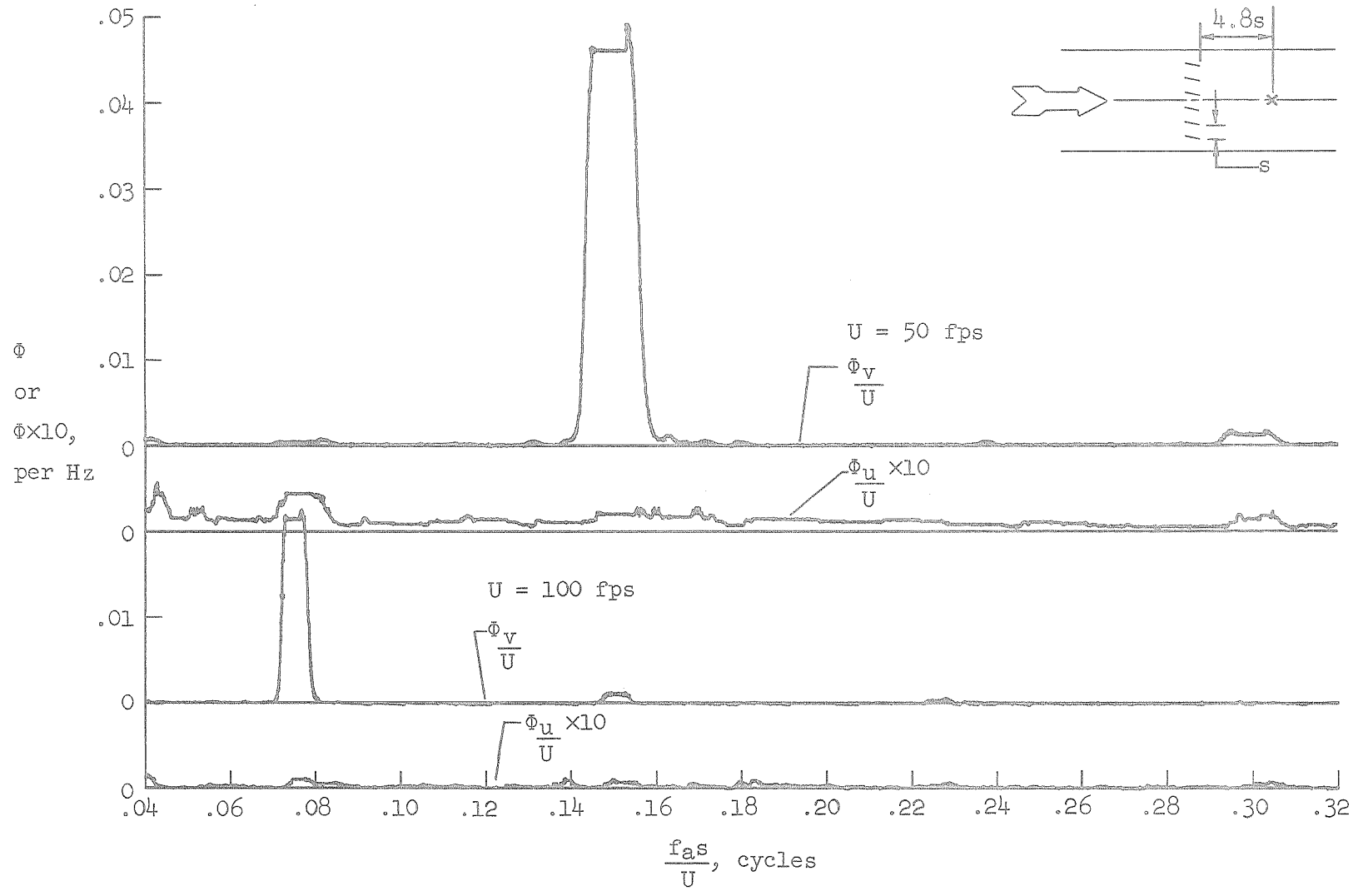

Figure 30.- Spectra of gusts at high fs/U on the channel centerline behind lateral-gust configuration A; $\alpha_{max} = 15°$.

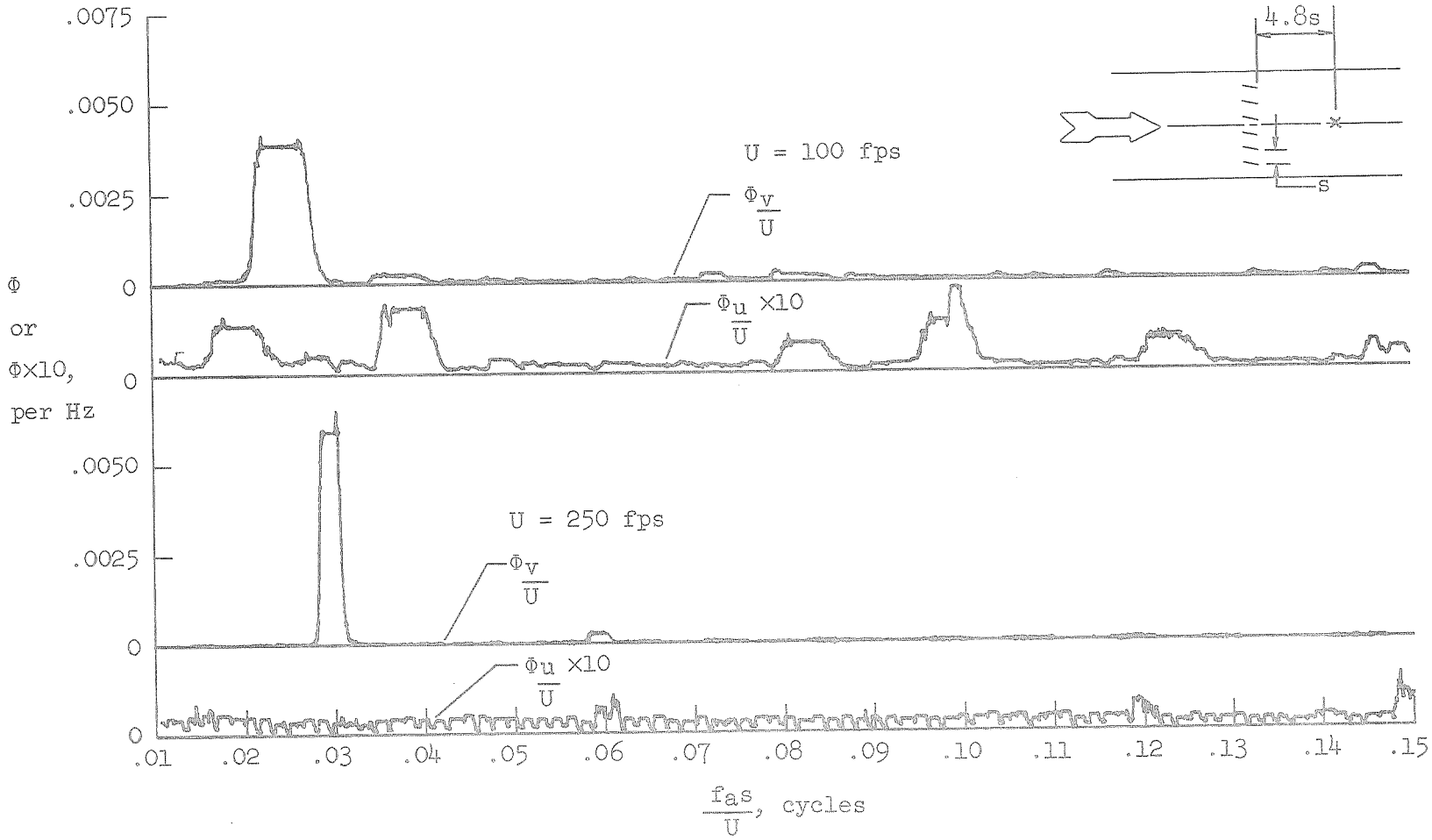

Figure 31.- Spectra of gusts at low fs/U on the channel centerline behind lateral-gust configuration A; $\alpha_{max} = 15^{\circ}$.

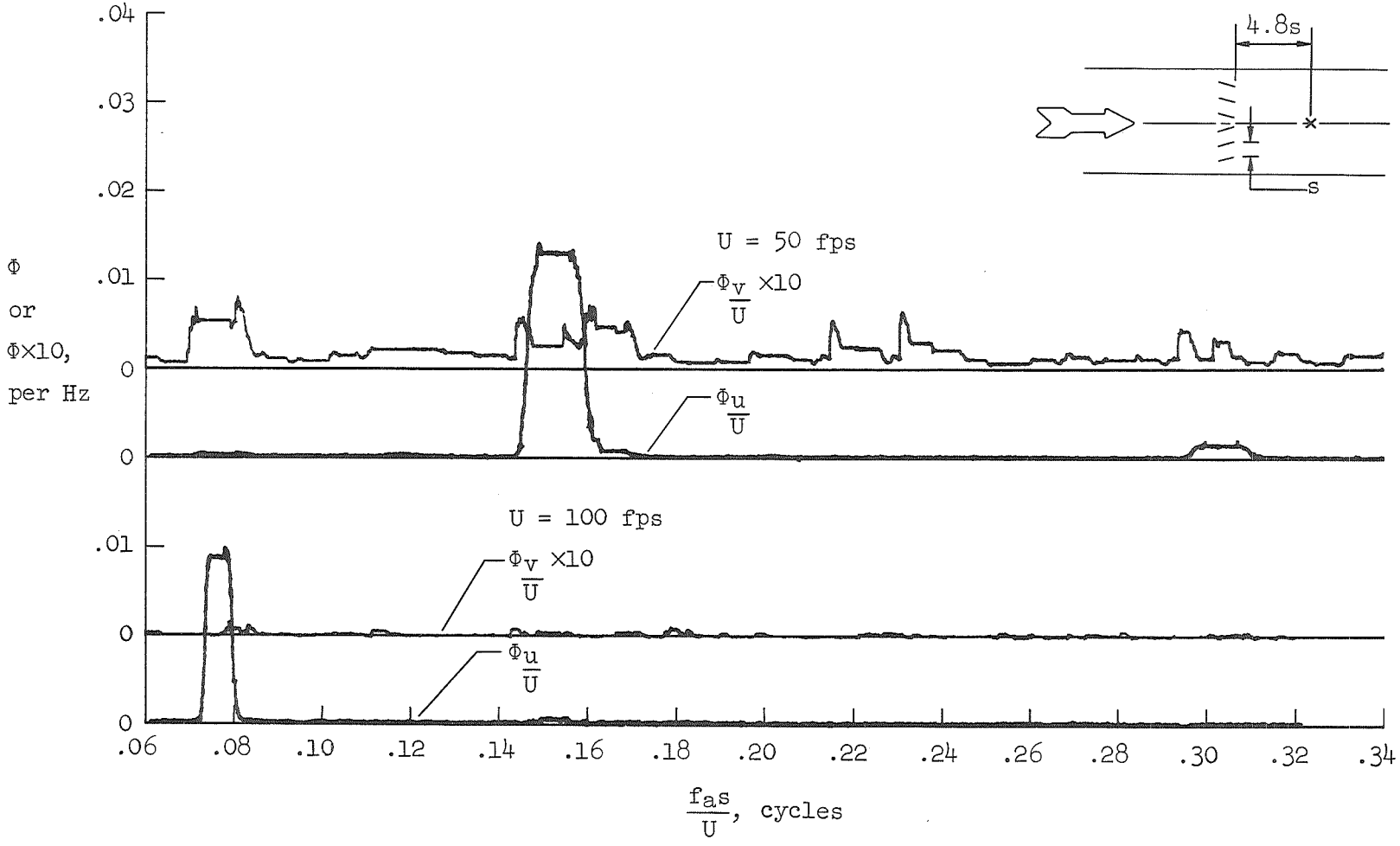

Figure 32.- Spectra of gusts at high fs/U on the channel centerline behind longiutudinal-gust configuration D; $\alpha_{max} \cong 12°$.

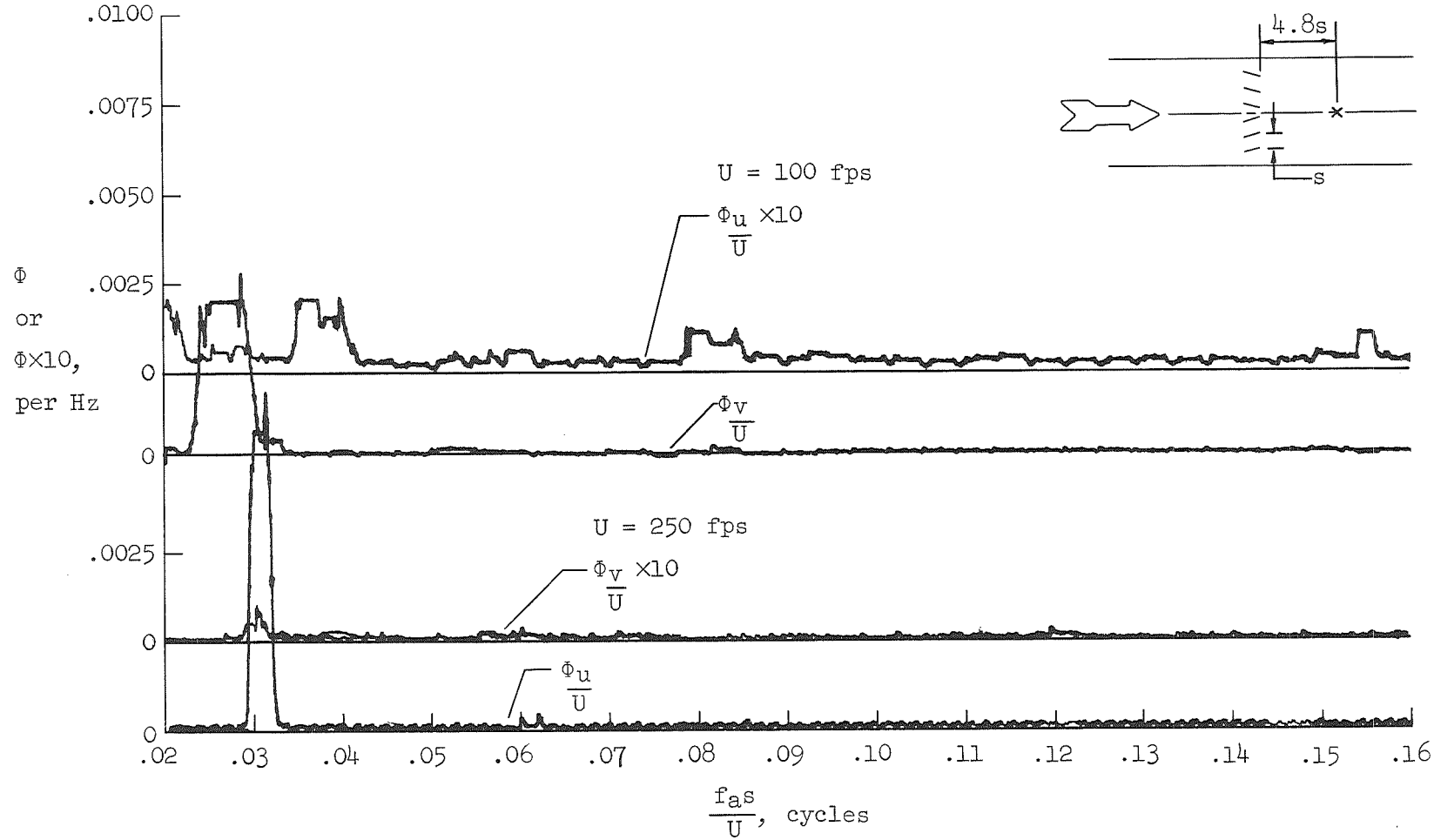

Figure 33.- Spectra of gusts at low fs/U on the channel centerline behind longitudinal-gust configuration D; $\alpha_{max} \cong 12°$.

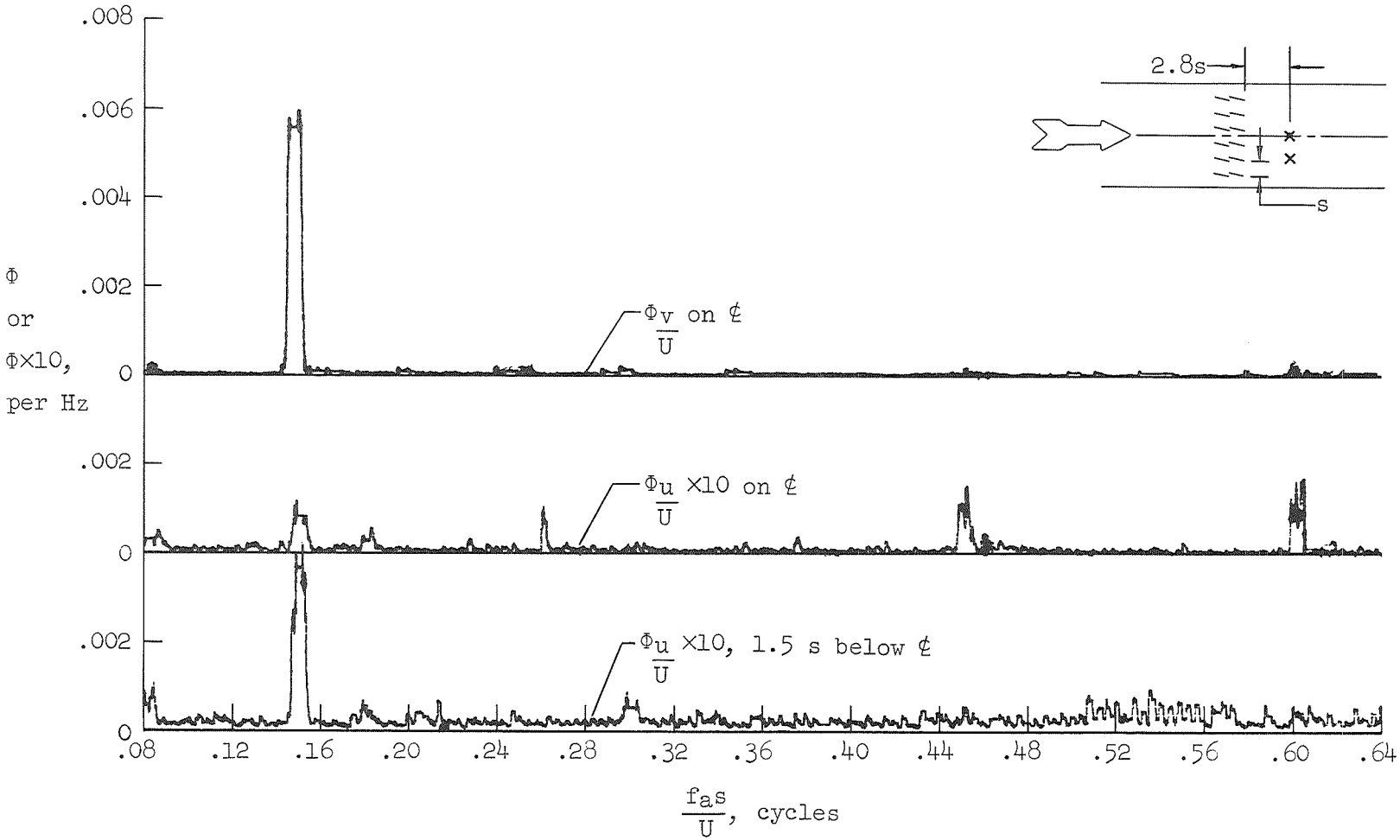

Figure 34.- Spectra of gusts at high fs/U at U = 100 fps behind lateral-gust configuration B; $\alpha_{max} \cong 3.50°$.

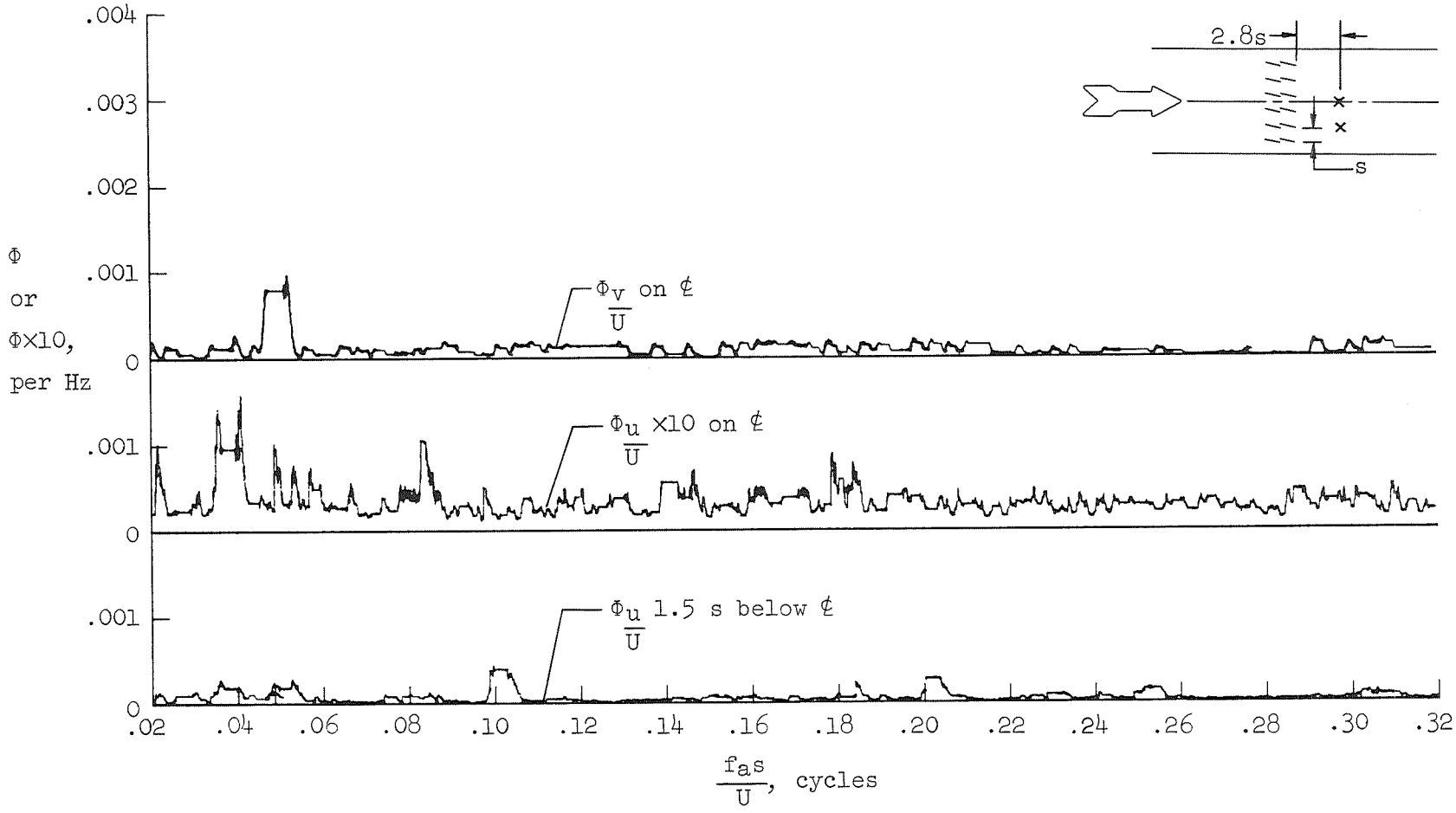

Figure 35.- Spectra of gusts at low fs/U at U = 100 fps behind lateral-gust configuration B; $\alpha_{max} \cong 3.50°$.

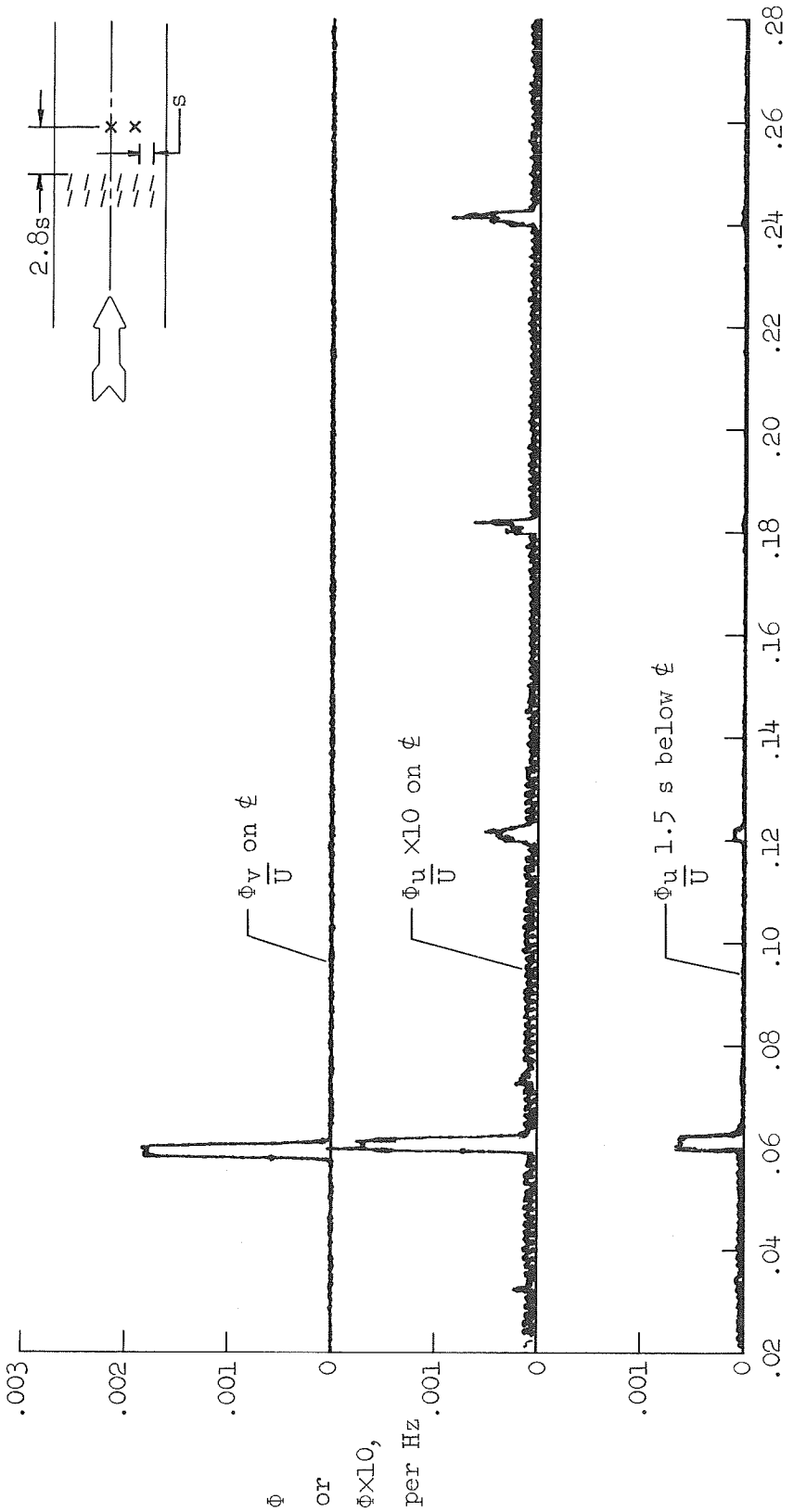

Figure 36.- Spectra of gusts at U = 250 fps behind lateral-gust configuration B; $\alpha_{max} \cong 3.50°$.

NASA-Langley, 1969 —— 11 A-3361

NATIONAL AERONAUTICS AND SPACE ADMINISTRATION
WASHINGTON, D. C. 20546
OFFICIAL BUSINESS

FIRST CLASS MAIL

POSTAGE AND FEES PAID
NATIONAL AERONAUTICS AN
SPACE ADMINISTRATION

POSTMASTER: If Undeliverable (Section 158
Postal Manual) Do Not Return

"The aeronautical and space activities of the United States shall be conducted so as to contribute . . . to the expansion of human knowledge of phenomena in the atmosphere and space. The Administration shall provide for the widest practicable and appropriate dissemination of information concerning its activities and the results thereof."

— NATIONAL AERONAUTICS AND SPACE ACT OF 1958

NASA SCIENTIFIC AND TECHNICAL PUBLICATIONS

TECHNICAL REPORTS: Scientific and technical information considered important, complete, and a lasting contribution to existing knowledge.

TECHNICAL NOTES: Information less broad in scope but nevertheless of importance as a contribution to existing knowledge.

TECHNICAL MEMORANDUMS: Information receiving limited distribution because of preliminary data, security classification, or other reasons.

CONTRACTOR REPORTS: Scientific and technical information generated under a NASA contract or grant and considered an important contribution to existing knowledge.

TECHNICAL TRANSLATIONS: Information published in a foreign language considered to merit NASA distribution in English.

SPECIAL PUBLICATIONS: Information derived from or of value to NASA activities. Publications include conference proceedings, monographs, data compilations, handbooks, sourcebooks, and special bibliographies.

TECHNOLOGY UTILIZATION PUBLICATIONS: Information on technology used by NASA that may be of particular interest in commercial and other non-aerospace applications. Publications include Tech Briefs, Technology Utilization Reports and Notes, and Technology Surveys.

Details on the availability of these publications may be obtained from:

SCIENTIFIC AND TECHNICAL INFORMATION DIVISION

NATIONAL AERONAUTICS AND SPACE ADMINISTRATION

Washington, D.C. 20546